Dissertation

Pediatric extremity computed tomography with focus on cone beam applications and radiation protection

submitted by

Dr.med.univ. Sebastian Tschauner

for the Academic Degree of

Doctor of Medical Science (Dr. scient. med.)

at the

Medical University of Graz

Department of Radiology, Division of Pediatric Radiology

under the Supervision of

Univ.-Prof. Dr.med.univ. Erich Sorantin

Assoc. Prof. Priv.-Doz. Dr.med.univ. Georg Singer

Univ.-Prof. Dr. Michael Riccabona

2019

Statutory declaration

I hereby declare that this thesis is my own original work and that I have fully acknowledged by name all of those individuals and organizations that have contributed to the research for this thesis. Due acknowledgment has been made in the text to all other material used. Throughout this thesis and in all related publications I followed the “Standards of Good Scientific Practice and Ombuds Committee at the Medical University of Graz.“

This thesis reproduces parts of the following publications, all authored by the doctoral candidate:

- **Tschauner S**, Marterer R, Nagy E, Apfaltrer G, Riccabona M, Singer G, Stücklschweiger G, Guss G, Sorantin E. Surface radiation dose comparison of a dedicated extremity cone beam computed tomography (CBCT) device and a multidetector computed tomography (MDCT) machine in pediatric ankle and wrist phantoms. PLoS One. 2017;12(6):e0178747. doi: 10.1371/journal.pone.0178747. PubMed PMID: 28570626.
- **Tschauner S** et al. Comparison of CBCT with MDCT / DR in pediatric extremity trauma. Publications in preparation and under review.

The following co-authors actively contributed to this dissertation and authorize the use of their personal data:

- Dr. Robert Marterer, Division of Pediatric Radiology, Department of Radiology, Medical University of Graz, Austria
- Dr. Eszter Nagy, Division of Pediatric Radiology, Department of Radiology, Medical University of Graz, Austria
- Dr. Georg Apfaltrer, Division of Pediatric Radiology, Department of Radiology, Medical University of Graz, Austria
- Univ.-Prof. Dr. Michael Riccabona, Division of Pediatric Radiology, Department of Radiology, Medical University of Graz, Austria
- Assoc. Prof. Priv.-Doz. Dr. Georg Singer, Division of General Paediatric and Adolescent Surgery, Department of Paediatric and Adolescent Surgery, Medical University of Graz, Austria

- Univ.-Prof. DDr. Erich Sorantin, Division of Pediatric Radiology, Department of Radiology, Medical University of Graz, Austria
- Mag. Helmuth Guss, MSc, Competence Centre for Medical Physics and Radiation Protection, University Hospital Graz, Graz, Austria
- Univ.-Doz. Mag. Dr. Georg Stücklschweiger, Competence Centre for Medical Physics and Radiation Protection, University Hospital Graz, Graz, Austria

Graz, 2019-07-23

Dedicated to

my beloved wife Krista

and my sons Markus and Alexander,

who sacrificed many hours and days of our mutual free-time

to support me in authoring this dissertation.

Acknowledgments

My studies would have been impossible without the continuous guidance and support of Univ.-Prof. Dr. Erich Sorantin. He always managed to pass on his passion for modern imaging, while embodying in-depth knowledge of pediatric pathophysiology and novel technical insights. His proactive approach to future challenges always motivated me during this project.

I also express my most profound appreciation to both other dissertation committee members, Assoc.-Prof. Dr. Georg Singer and Univ.-Prof. Dr. Michael Riccabona. As renowned experts in their disciplines, they provided assistance and advice in many respects.

My thanks go to all my other colleagues who took part in the course of the studies, especially Dr. Robert Marterer and Dr. Eszter Nagy.

I thank Doz. Dr. Georg Stücklschweiger and his team from the Competence Centre for Medical Physics and Radiation Protection, University Hospital Graz for their assistance with the surface dose measurements.

I also thank the company Braincon GmbH & Co KG (Grinzinger Allee 5, 1090 Vienna, Austria) for providing our University Hospital Graz (Auenbruggerplatz 1, 8036 Graz, Austria) with the Planmed Verity® test sample used in this dissertation.

Last but not least, I am deeply indebted to my parents Doris and Christian, who laid the foundation for my medical career by giving all their support, liberties and time to develop my ideas, which I am ever more thankful.

Thanks for all your support!

Table of Contents

Statutory declaration I

Acknowledgments IV

Table of Contents V

Abbreviations and Definitions VIII

List of Figures X

List of Tables XI

Abstract in German XII

Abstract in English XIV

1. Introduction 1

  1.1. History of CBCT 2

  1.2. Similarities and differences between CBCT and MDCT 2

    1.2.1. CBCT image acquisition 4

    1.2.2. CBCT image reconstruction 4

    1.2.3. CT-related image artifacts 4

  1.3. Extremity CBCT devices 7

  1.4. Extremity CT indications in children 8

2. Material and Methods 11

  2.1. Study CT scanners 11

    2.1.1. CBCT 11

    2.1.2. MDCT 12

  2.2. Phantoms 13

    2.2.1. Dosimeters 14

  2.3. Patients 15

    2.3.1. Patients receiving CBCT 15

    2.3.2. Patients undergoing MDCT 15

    2.3.3. Patients sustaining DR 16

2.4. Image acquisition 18
2.4.1. Phantom scanning settings 18
2.4.2. Patient scanning settings 19
2.5. Image analyses 21
2.5.1. Semi-objective image analysis 21
2.5.2. Subjective image impression 23
2.5.3. Comparison of CBCT and DR 23
2.6. Statistical analyses 24
2.7. Ethics committee 24
3. Results 25
3.1. Phantom surface dose assessment 25
3.2. Comparison of CBCT and DR 30
3.3. Comparison of CBCT and MDCT 31
4. Discussion 37
4.1. Related literature 38
4.1.1. Comparable studies 38
4.1.2. Related studies in adults and phantoms 39
4.1.3. Review literature 41
4.2. Radiation dose considerations 41
4.3. Image quality-related aspects 42
4.3.1. Greyscale values in CBCT 44
4.3.2. Soft tissue visualization 44
4.3.3. Iterative reconstruction 45
4.3.4. Scout images 45
4.4. CBCT-specific features 46
4.4.1. Device mobility 46
4.4.2. Weight-bearing 46

4.4.3. Lead curtain shield 47
4.5. Limitations 47
5. Conclusions 49
Bibliography.. 50

Abbreviations and Definitions

AIDR3D	Adaptive Iterative Dose Reduction using Three Dimensional Processing
ALARA	As low as reasonably achievable
ASIR	Adaptive statistical iterative reconstruction
AUC	Area under the curve
CE	Contrast-enhanced
CI	Confidence interval
CCD	Charge-coupled device
CMOS	Complementary metal-oxide-semiconductor
CT	Computed tomography
CBCT	Cone beam computed tomography
DICOM	Digital Imaging and Communications in Medicine
DR	Digital radiography
FBP	Filtered back projection
FOV	Field of view
MBIR	Model-based iterative reconstruction
MDCT	Multidetector computed tomography
mSv	Millisievert
$CTDI_{vol}$	CT dose index
DLP	Dose length product
HU	Hounsfield unit

ICRP	International Commission on Radiological Protection
ID	Identifier
LiF	Lithium fluoride
MPR	Multiplanar reconstruction
MRI	Magnetic resonance imaging
ROI	Region of interest
SD	Standard deviation
TLD	Thermoluminescent dosimeter
WB	Weight-bearing

List of Figures

Figure 1 Schematic comparison of CBCT and MDCT. 3
Figure 2. Selected examples of various common CT image quality measures and artifacts. 7
Figure 3. Comparison of the entire extremity CT and radiograph numbers per year in the author's institution. 9
Figure 4. The yearly number of extremity MDCT examinations at the author's institution. 9
Figure 5. CBCT (on the right) and MDCT (on the left) next to each other. 12
Figure 6. Ankle (above) and wrist (below) phantom in the gantry of the CBCT. ... 13
Figure 7. TLDs attached in clockwise positions around the pediatric wrist phantom. 15
Figure 8. Flowchart of the study design. 17
Figure 9. Histogram of a sample axial CT stack. 22
Figure 10. Box plots of surface radiation doses. 27
Figure 11. A Bland-Altman plot depicts test-retest reliability of the conducted surface dose analyses in the pediatric ankle and wrist phantoms. 30
Figure 12. ROC curves of both observers 31
Figure 13. Semi-objective image quality parameters compared between CBCT and MDCT 32
Figure 14. Subjective image impression ratings. 33
Figure 15. Example of a Tillaux fracture of the distal left tibia in an anteroposterior DR of the ankle (left), in a coronal reformat of the CBCT (middle), and MDCT (right). 37
Figure 16. Side-by-side samples of CBCT and MDCT of corresponding patients. 39
Figure 17. Imaging of the wrist of a 17-year-old adolescent with a fracture of the trapezoid bone. 40
Figure 18. Examples of typical artifacts observed in CT examinations. 43

List of Tables

Table 1. Exposure parameters for scanning phantoms of the ankle and wrist. 19
Table 2. Exposure parameters and reconstruction settings of both study devices for patient scanning. 20
Table 3. Results of surface dose measurements between CBCT and MDCT (routine). 26
Table 4. Collected dose measurements (mGy) displayed for both devices, both phantoms, and all used protocol settings (21). 28
Table 5. A consensus rating of image quality in the pediatric ankle and wrist phantoms 29
Table 6. Subjective image interpretation. 35

Abstract in German

Hintergrund:

Neuartige dedizierte Cone-beam Computertomographie-Geräte (CBCT) zur Untersuchung der Extremitäten sind seit wenigen Jahren verfügbar. Sie stellen eine mögliche Alternative zu den üblicherweise zur weiterführenden Traumadiagnostik verwendeten Multidetektor-Computertomographen (MDCT) dar. Entsprechende wissenschaftliche Literatur über den Einsatz von CBCT beim kindlichen Extremitätentrauma ist rar gesät. Das Ziel dieser Arbeit war daher, die neue und die etablierte Methode miteinander zu vergleichen, sowie die Vor- und Nachteile in einem möglichst realitätsnahen kinderradiologischen Umfeld herauszuarbeiten.

Material und Methoden:

Wir führten Oberflächendosismessungen an kindlichen anthropomorphen Hand- und Sprunggelenksphantomen durch und fertigten prospektiv CBCT-Untersuchungen von Extremitäten verletzter Kinder an.

Die Phantomstudie erfolgte mittels Thermoluminiszenzdosimetern, welche an den Phantomen angebracht wurden. Dann wurden diese mehrfach mit verschiedenen Belichtungsprotokollen an CBCT und MDCT untersucht und die Dosimeter anschließend ausgewertet.

Im Studienzeitraum konnten prospektiv 61 Extremitäten-CBCTs von 59 Patientinnen und Patienten akquiriert werden, 10 davon wurden zusätzlich mit MDCT untersucht, um einen direkten Vergleich zu ermöglichen. Die restlichen 51 MDCTs wurden anhand Untersuchungsregion, Geschlecht und Alter retrospektiv aus dem lokalen Bildarchiv zugeordnet. 7 Untersuchungspaare mussten ausgeschlossen werden, da bei Gipsverbänden oder Metallimplantaten Diskrepanzen zwischen den Modalitäten vorlagen. Insgesamt wurden 54 CBCT-MDCT-Paare eingeschlossen.

Zusätzlich erfolgte eine vergleichende Gegenüberstellung der diagnostischen Aussagekraft von digitalen Röntgenaufnahmen (DR) zu CBCTs an 47 korrespondierenden Untersuchungspaaren.

Resultate:

Die Messungen der Oberflächendosen an Hand- und Sprunggelenksphantomen zeigten im Mittel einen signifikanten Dosisvorteil der CBCT gegenüber der MDCT (3,0 Milligray bzw. 3,9 Milligray, $p<0{,}001$).

Erwartungsgemäß zeigte sich im Vergleich von CBCT und DR ein Vorteil für die Schnittbildgebungsmethode, welche eine höhere Anzahl an Frakturen erkennen konnte. Die Sensitivität lag hierbei zwischen 88,5% und 92,3% in der CBCT und bei 65,4% in der DR.

In der Gegenüberstellung von CBCT und MDCT fand sich bei ersterer ein vorteilhafteres Rauschverhalten, sowohl semi-objektiv als auch subjektiv ($p<0{,}001$). Die CBCT-Untersuchungen waren allerdings regelmäßig durch Streifenartefakte beeinträchtigt, wodurch sich subjektiv die diagnostische Sicherheit reduzierte ($p=0.001$).

Schlussfolgerungen:

Bei Kindern bot die speziell für Extremitätenbildgebung bestimmte CBCT semi-objektiv gemessen eine höhere Bildqualität als vergleichbare MDCT-Untersuchungen. Im Gegenzug wurden die subjektive Bildqualität und die diagnostische Aussagekraft der CBCT schlechter bewertet, was insbesondere auf das Vorliegen von Streifenartefakten zurückgeführt werden konnte. Außerdem war die CBCT anfälliger gegenüber Bewegungsartefakten, wenngleich diese insgesamt selten gesehen wurden. Bei Verwendung optimierter Belichtungsprotokolle bewegten sich die applizierten Strahlendosen beider Methoden (CBCT und MDCT) im niedrigen Bereich weniger Tage natürlicher Hintergrundstrahlung und spielten daher in Hinsicht auf pädiatrische Traumaanwendungen bei strikter Indikationsstellung eine untergeordnete Rolle.

Abstract in English

Background:

Novel dedicated cone-beam computed tomography (CBCT) devices for examining the extremities have been available for a few years. They represent a possible alternative to the multidetector computed tomography (MDCT) machines commonly used for further trauma diagnostics. The corresponding scientific literature on the use of CBCT in childhood extremity trauma is scarce. The aim of this work was therefore to compare the new and the traditional method to identify the specific advantages and disadvantages in a realistic pediatric radiological setting.

Material and Methods:

We performed surface dose measurements on pediatric anthropomorphic hand and ankle phantoms and prospectively acquired CBCT examinations of the extremities of injured children.

The phantom study was carried out utilizing thermoluminescence dosimeters, which were attached to the phantoms. Then they were irradiated several times with different exposure protocols on CBCT and MDCT. The dosimeters were subsequently read out.

During the study period, 61 limb CBCTs were obtained from 59 patients prospectively, 10 of whom were additionally scanned with MDCT in parallel to allow a direct comparison. The remaining 51 MDCTs were retrospectively matched by examined region, gender, and age from the local image archive. Seven examination pairs had to be excluded, as there were discrepancies between the modalities concerning plaster casts or metal implants. A total of 54 CBCT-MDCT pairs were included.

Besides, an analysis of the diagnostic value of digital radiography (DR) compared to CBCTs was performed on 47 corresponding examination pairs.

Results:

Measurements of surface doses on hand and ankle phantoms showed a significant dose advantage of CBCT over MDCT (3.0 milligray and 3.9 milligray, $p<0.001$, respectively) on average.

As expected, CBCT and DR demonstrated an advantage of the sectional imaging technique, which was able to detect a higher number of fractures. Sensitivity was between 88.5% and 92.3% in CBCT and 65.4% in DR.

When comparing CBCT and MDCT, the former showed a more favorable noise characteristic, both semi-objectively and subjectively ($p<0.001$). However, CBCT examinations were regularly affected by streak artifacts, which subjectively reduced diagnostic certainty ratings ($p=0.001$).

Conclusions:

In children, CBCT which was designed explicitly for extremity imaging semi-objectively performed better than the comparable MDCT. On the other hand, the subjective image quality and the diagnostic certainty of CBCT were rated worse, which could be attributed in particular to the presence of streak artifacts. Also, CBCT was more susceptible to motion artifacts, although they were rarely seen. Using optimized exposure protocols, the administered radiation doses of both methods (CBCT and MDCT) were in the low range of a few days of natural background radiation and therefore played a minor role in pediatric trauma setting with strict study indications.

1. Introduction

Modern extremity imaging would be hardly conceivable without computed tomography (CT), which is also true in the pediatric population (1-5). Especially since the introduction of multidetector CT (MDCT) in the late 1990s (6, 7), CT has started its worldwide triumph, and most current diagnostic pathways are highly dependent on this modality (2). In children, there still is a more limited set of CT indications (8, 9) due to relatively high necessary doses and the resulting concern for radiation-induced damage in later life. Recent studies on large populations additionally fueled these worries about radiation effects, especially concerning carcinogenesis (10-13). However, actual patient risks of low-dose exposures applied by CT examinations stay a topic of contentious debates and ongoing research (11).

Lately, a limited set of dedicated extremity cone beam computed tomography (CBCT) devices became available for clinical use (14-16). They offer comparably compact sizes, machine mobility and promise a lower radiation dose at superior image quality (17, 18). However, CBCT (synonyms: C-arm CT, cone beam volume CT, or flat panel CT, digital volume tomography) machines still have to prove their advantages over MDCT regarding image characteristics and radiation dose properties, especially as currently available studies are partially inconsistent. Data in pediatric populations are particularly scarce (19-21).

Apart from a broad spectrum of operational areas in dentistry and facial surgery (22-29), radiotherapy (30-35) and intraoperative guidance (36-42), as well as a variety of interventional applications (43-79) the method still did not gain adequate traction in other fields of diagnostic imaging. Regarding extremity imaging, mainly weight-bearing CBCT received some attraction in the recent literature (80-87). Though, the authors of a current review on non-dental CBCT applications stated the limited availability and heterogeneity of data on this topic, which rendered a meta-analysis in their paper impossible (88).

1.1. History of CBCT

The idea of CBCT is probably as old as computed tomography itself, inspired by the possibility to complete a CT examination with a single X-ray tube rotation or less (89). First attempts to build a CBCT machine can be dated back to the 1970s with the “dynamic spatial reconstructor” created by the Biodynamics Research Unit at the Mayo Clinic (90-95) but did not lead to significant clinical use (89). The primary hurdle in the development was the absence of proper detectors with large-enough areas and sufficient dynamic ranges, which were not available until the late 1990s (89). Meanwhile attempts to build CBCT machines using image intensifier equipment were unsuccessful (89).

For several decades, the development of CBCT and conventional single and multiple slice CT took two segregated paths. However, with the evolution of multidetector CT and increasingly broader detectors with more and more added detector rows, the initially used fan-shaped geometry in MDCT re-approached to a cone-beam geometry that both methods employ these days. As third and fourth generation MDCT scanners also use cone beam X-rays, the term CBCT is commonly referred to systems that specifically use any flat-panel detector (89). The term CBCT is also used in the context of flat-panel CT throughout this dissertation.

Development of the first commercial CBCT started in the mid-1990s in Italy (96). It was first introduced in the European market in 1996 by the company “QR s.r.l.” with the “NewTom 9000” for dental applications (97-99).

1.2. Similarities and differences between CBCT and MDCT

CBCT and MDCT images exhibit a similar image impression, and particularly non-experienced viewers will struggle to discriminate between the modalities reliably. Thus, the fundamental differences between modern CBCT and MDCT machines may not be apparent at first glance.

Both technologies employ a cone-shaped Roentgen beam produced by their X-ray tubes, rotating around the examined body region (89, 100, 101). They mainly differ concerning detector technology. CBCT scanners are typically fitted with flat-panel detectors (102-104) with equispatial geometry (105), including amorphous silicon, charge-coupled device (CCD) and complementary metal-oxide-semiconductor (CMOS) detectors (89). They offer small pixel sizes and therefore fine-grained acquired images, which enable CBCT to achieve superior spatial image resolution, while on the other hand making it prone to scatter artifacts (106-111). Another disadvantage of CBCT-detectors is a relatively lower dynamic range that is aggravated by a usually smaller X-ray generator performance. Together, the result is an only mediocre soft tissue contrast.

MDCT scanners, on the other hand, are equipped with curved equiangular detectors in multiple rows (112) and pre-detector anti-scatter lamella. Figure 1 schematically shows the explained similarities and differences.

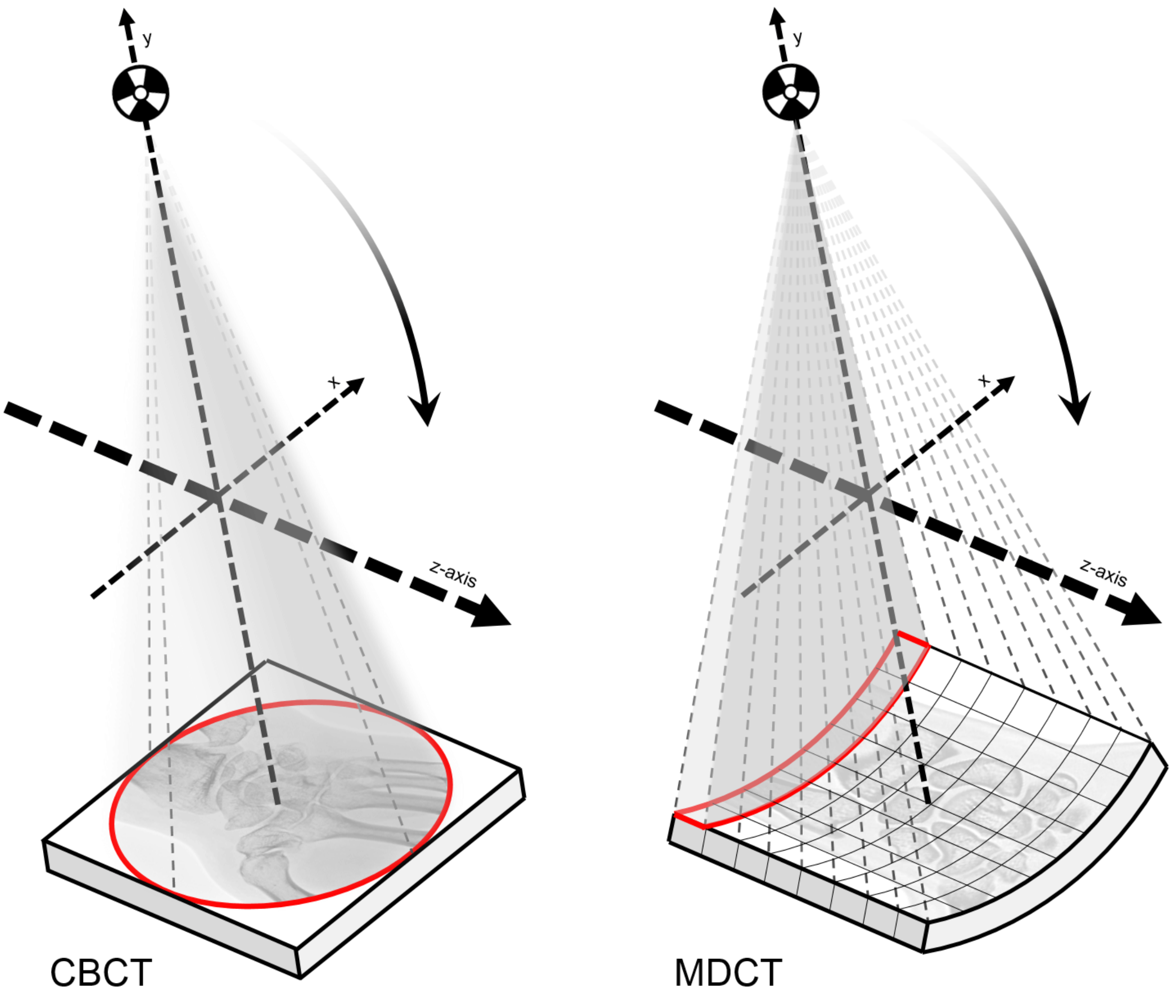

Figure 1 Schematic comparison of CBCT and MDCT. CBCT uses a flat-panel detector to generate multiple projection images from different angles, while MDCT combines multiple detector slices (eight are shown in this example) to an image

series. For a better visibility, only one fan-shaped detector row is accentuated. Modified from Miracle et al. (open access) (113).

Due to the more straightforward build, CBCT manufacturers can construct smaller form factor machines. This compactness also enables the design of mobile devices that allow new use cases.

1.2.1. CBCT image acquisition

During CBCT examinations, an X-ray tube and a flat panel detector rotate opposite from each other, mounted on a C-shaped arm, or built in a gantry. The machines take multiple projections from different angles, usually ranging between 20 and 40 seconds for acquiring a complete volume of the examined body region. Manufacturers often use incomplete gantry rotations less than 360 degrees. Typically, the devices make a few hundred two-dimensional high-resolution projection images.

1.2.2. CBCT image reconstruction

Image reconstruction is usually based on a modified Feldkamp algorithm (114). The above-mentioned projection image set of the examined body part serves as a basis for the following reconstruction of a three-dimensional volume, which usually consists of isotropic voxels. Isotropic means that the voxels feature identical dimensions in all three spatial directions, enabling high-resolution multi-planar reconstructions (= MPRs).

1.2.3. CT-related image artifacts

The term *artifact* is etymologically derived from the Latin words “ars” (skill) and “facere” (to make) (115, 116). In a radiological context, artifacts refer to systematic errors in image generation, resulting in studies that partly or entirely do not reflect the real patient anatomy or tissue attenuation (101, 117). These artificially generated effects can impair the validity of a radiological report, or even make diagnosing impossible. A radiologist, therefore, needs to be able to know, recognize and interpret the numerous possible artifacts that may occur at every step of image acquisition, reconstruction, and post-processing (101).

CBCT and MDCT suffer from similar types of artifacts. They are usually differentiated into categories based on the principle of their origin, further described and discussed in the following paragraphs.

1.2.3.1. Physics-related artifacts

Artifacts related to physical effects are strongly linked to the type and construction of a CT scanner and the chosen exposure parameters while scanning (101). A brief selection of the essential physics-related artifacts is presented below.

Imaging systems are only theoretically free of internal impairments resulting in **noise**. These inherent errors are small in modern CT scanners, making the so-called “quantum noise” caused by the variations in X-ray photons reaching the detector the principal cause of image noise (101).

X-ray beams consist of photons with different energy levels. Irradiated tissues absorb lower-energy photons quicker, causing the X-ray beam to be composed of higher energy components, referred to as “**beam hardening**.” The results are “cupping artifacts,” where X-rays in the middle of an object are attenuated more severely than peripherally, and “streak artifacts,” where information is lost between two or more radiodense structures (111, 117).

Very dense structures can stop an X-ray beam, preventing photons from reaching the detector, referred to as “**photon starvation**.” Photon starvation causes streak artifacts, commonly seen behind metal implants (117, 118).

Partial volume artifacts increase the thicker an image slice is reconstructed from the raw dataset, relevant for objects that partially reach into, or are thinner than the reconstruction plane (101). These artifacts were common in the early days of CT. In modern extremity CT, reconstructed slice thicknesses of 1 mm and lower prevent partial volume effects almost entirely because thin multiplanar reconstructions became standard (101).

Aliasing in CT images manifests as thin radiating streaks and reticulated patterns that diverge outwards. In image reconstruction, a voxel’s brightness is calculated from multiple angle views. In cases of insufficient numbers of acquired projections, also known as “undersampling,” an erroneous brightness may be calculated, resulting in aliasing artifacts (89, 101).

1.2.3.2. Patient-related artifacts

The main patient-dependent artifact during image acquisition is motion, including breathing and pulsation. Motion artifacts can be avoided by decreasing acquisition time in terms of higher rotation speeds and avoidance of table increment (119) or mathematical compensation procedures in image reconstruction (120-122). Fast acquisition times are typically available on modern MDCT scanners with large detectors, which counteract susceptibility to patient motion.

Flow-artifacts can principally occur in contrast-enhanced (CE) examinations and may degrade the depiction of vessels. As CT in pediatric extremity trauma usually is performed without contrast, the effect is of minor relevance.

Radiopaque materials (like for example metal implants) within the scan area commonly result in major streak artifacts, described before in more detail in the paragraph photon starvation (117).

1.2.3.3. Hardware-related artifacts

Ring artifacts of different intensities may occur due to uncalibrated or defect detector elements (117). When visible, detectors usually are quickly re-calibrated, or, if not successful, need to be repaired (123); thus, we do not see ring artifacts frequently in routine.

Out of field artifacts typically occur when a part of the patient is outside the scan field. Due to the partially missing information, the reconstruction will lead to artifacts, especially in off-centered regions (117).

Tube arcing artifacts are rare, caused by an intermittent short circuit between the anode and the cathode of the X-ray tube. It results in a unique form of streak artifact (124).

Windmill artifacts are a type of streak artifact from helical scanning, pronounced in examinations with high pitch settings. Usually, they are of no relevance in pediatric extremity CBCT and MDCT, often performed with no or low pitch (117).

MPR (multiplanar reformation) artifacts occur when image planes are reconstructed from non-isotropic voxels (117), which is of no relevance in any modern CBCT or MDCT scanner.

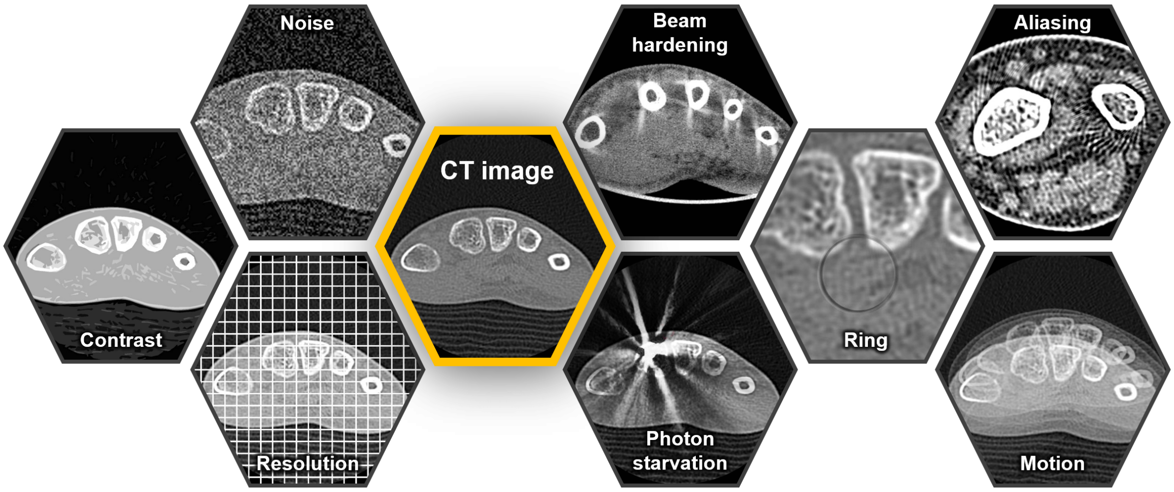

Figure 2. Selected examples of various common CT image quality measures and artifacts. The primary image quality criteria resolution, contrast, and noise are shown on the left, artifacts on the right half of the figure.

1.2.3.4. Software-related artifacts

Image reconstruction and post-processing may introduce plenty of possible artifacts due to image manipulation. None of these artifacts are typical or common, and they do not demand further discussion in the context of pediatric extremity CT applications.

1.3. Extremity CBCT devices

A limited number of dedicated CBCT devices for extremity scanning is commercially available at the time of writing:

- Carestream OnSight 3D (Carestream Health, Inc., Rochester, New York, USA, https://www.carestream.com) (14, 84, 125)
- CurveBeam InReach™, LineUp™ and pedCAT™ (CurveBeam, Warrington, Pennsylvania, USA, https://www.curvebeam.com) (126)
- Planmed Verity™ (Planmed Oy, Helsinki, Finland, https://www.planmed.com) (17, 18, 127)

They provide similar features like small build, movability, and possibilities to perform examinations under weight-bearing.

1.4. Extremity CT indications in children

As mentioned before, pediatric CT examinations require strict indications (11, 12). Referrer and radiologist have to select patients profiting from this cross-sectional imaging method carefully. CT studies are therefore primarily performed in cases of complicated, comminuted and intraarticular fractures, or in regions where radiographs poorly depict fractures and in cases of suspected bone tumors. Preceding X-rays in two or more planes are still the basis of decision-making for CT in almost all cases sent to our pediatric radiology division.

Specifying the term extremity imaging (CT, radiography) in this manuscript, lower extremity refers to all regions including the thigh distally (thigh, knee, lower leg, ankle, foot, toes) and upper extremity to the upper arm distally (upper arm, elbow, forearm, wrist, hand, fingers).

In a data analysis of the local pediatric radiology division's examinations, we saw a moderate relative increase in extremity trauma radiographs by 16% since 2007. In contrast, the amount of corresponding trauma CTs rose by 274% in the same period. Approximately 1% of our extremity trauma patients receive an MDCT today, which steadily increased from 0.3% ten years ago. Figure 3 depicts these findings.

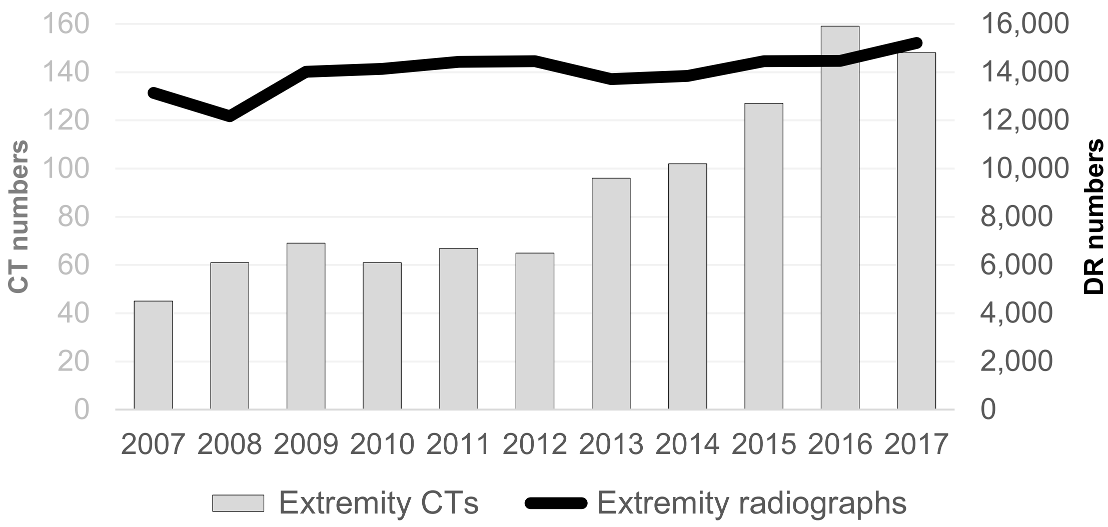

Figure 3. Comparison of the entire extremity CT and radiograph numbers per year in the author's institution. The line shows the number of extremity radiographs per year, while the bars represent the amount of corresponding CTs with a relative increase in the last years.

Concerning body regions, lower extremity CT studies were relatively more frequent than the upper extremity. However, the gap between them decreased (compare Figure 4). Regarding the upper extremity CTs, elbow study numbers increased the most.

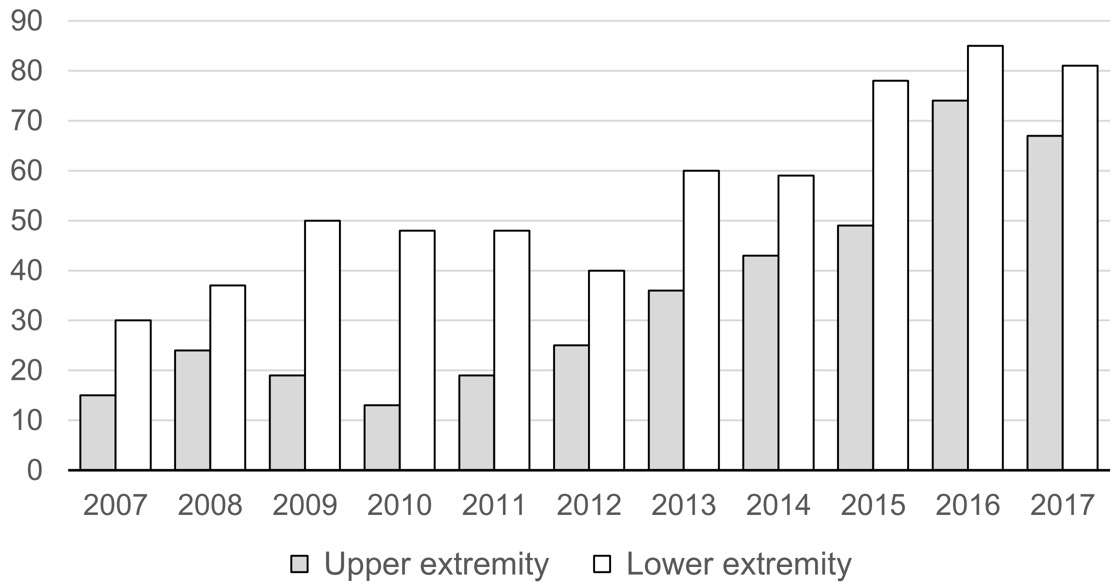

Figure 4. The yearly number of extremity MDCT examinations at the author's institution. Grey bars represent the upper, white bars the lower limb. An increase in the number of examinations is obvious.

Regarding study indications, pediatricians and pediatric surgeons indicated nearly 5% of all CTs in the context of possible or definite bone tumors and pathological fractures. About 9% of CTs were performed based on orthopedic questions like tarsal coalitions or osteochondral lesions. The remaining vast majority of studies was related to acute trauma or trauma complications.

The fundamental hypothesis of this dissertation was that dedicated pediatric extremity CBCT should achieve higher image quality measures when compared to its direct competitor, MDCT. Semi-objective study quality, subjective image impression, and surface radiation dose served as the relevant parameters to address that statement. We additionally hypothesized a potentially more elevated amount of motion artifacts in CBCT, due to comparatively longer acquisition times. Another topic of interest was the evaluation of image artifacts compared between the CT modalities. To proof these conjectures, we performed experiments on extremity phantoms and injured pediatric patients at a tertiary center for pediatric radiology and traumatology.

2. Material and Methods

We conducted side by side image quality assessments and dose measurements of a CBCT and an MDCT scanner in anthropomorphic phantoms and assessed a pediatric trauma patient sample in this single-center prospective study.

2.1. Study CT scanners

Radiographers acquired all study-related images on a novel dedicated extremity CBCT device, and a modern MDCT equipped with the latest dose-saving application. Both of the compared machines represent state of the art technology with the MDCT currently known as the gold standard for many, but not all pediatric trauma indications (9, 128-130).

2.1.1. CBCT

A Verity™ scanner (Planmed Oy, Helsinki, Finland) was used to acquire the CBCT images (compare Figure 5). This device consists of a small gantry mounted on a movable framework. The gantry itself can be tilted and height-adjusted to fit the investigated region. As a consequence, studies under weight-bearing are possible. In this study, patients were positioned on a seat next to the gantry opening. The examined body part was then centered in the middle of the gantry, as indicated by the laser position markers. The acquired cylindrical field of view (FOV) was 12 or 6 cm proximo-distally with a diameter of 16 cm. Standard examination protocols were analyzed and exposure parameters lowered by one third on average. The prefabricated unchangeable acquisition time was 36 seconds. CBCT tube rotation angle was 210°. As recommended, the included lead curtain shield (131) was used in addition to the routinely applied body shielding whenever possible (21).

Figure 5. CBCT (on the right) and MDCT (on the left) next to each other. The CBCT device was kept in the MDCT scanner room exclusively, as local regulations require a radio-protected facility for operation. The associated seat is not shown in this photograph.

2.1.2. MDCT

Radiological technologists conducted the study-related MDCT examinations on a Toshiba Aquilion One (Toshiba Medical Systems Corporation, Otawara-shi, Japan), shown in Figure 5. This device equipped with the latest software and hardware updates had been in use at the author’s institution since 2008. The MDCT detector can acquire 320 rows of 0.5 mm collimated slices, covering a maximum scan range of 16 cm per single tube rotation (2). The injured extremity was centered in the gantry as efficiently as possible before scout images were obtained before every volumetric image acquisition. Dose-optimized pediatric MDCT protocols were used in all patients. There were no adaptions to these routinely employed protocols for this study. Proximo-distal extension varied from 10 to 16 cm. Tube rotation time was 0.5 seconds. MDCT examinations were done without table movement (pitch) within one 360 degrees tube rotation (21).

2.2. Phantoms

We conducted the dosimetric studies with the aid of the left lower leg and the right forearm of the pediatric whole-body phantom “PBU-70” (Kyoto Kagaku Co. Ltd, Kyoto, Japan) (132), resembling a 4-year-old child (height = 105 cm, weight = 20 kg). The phantom extremities consisted of cortical and trabecular bone, embedded in soft tissue-like material. Figure 6 shows both phantoms placed on the gantry of the CBCT scanner (21).

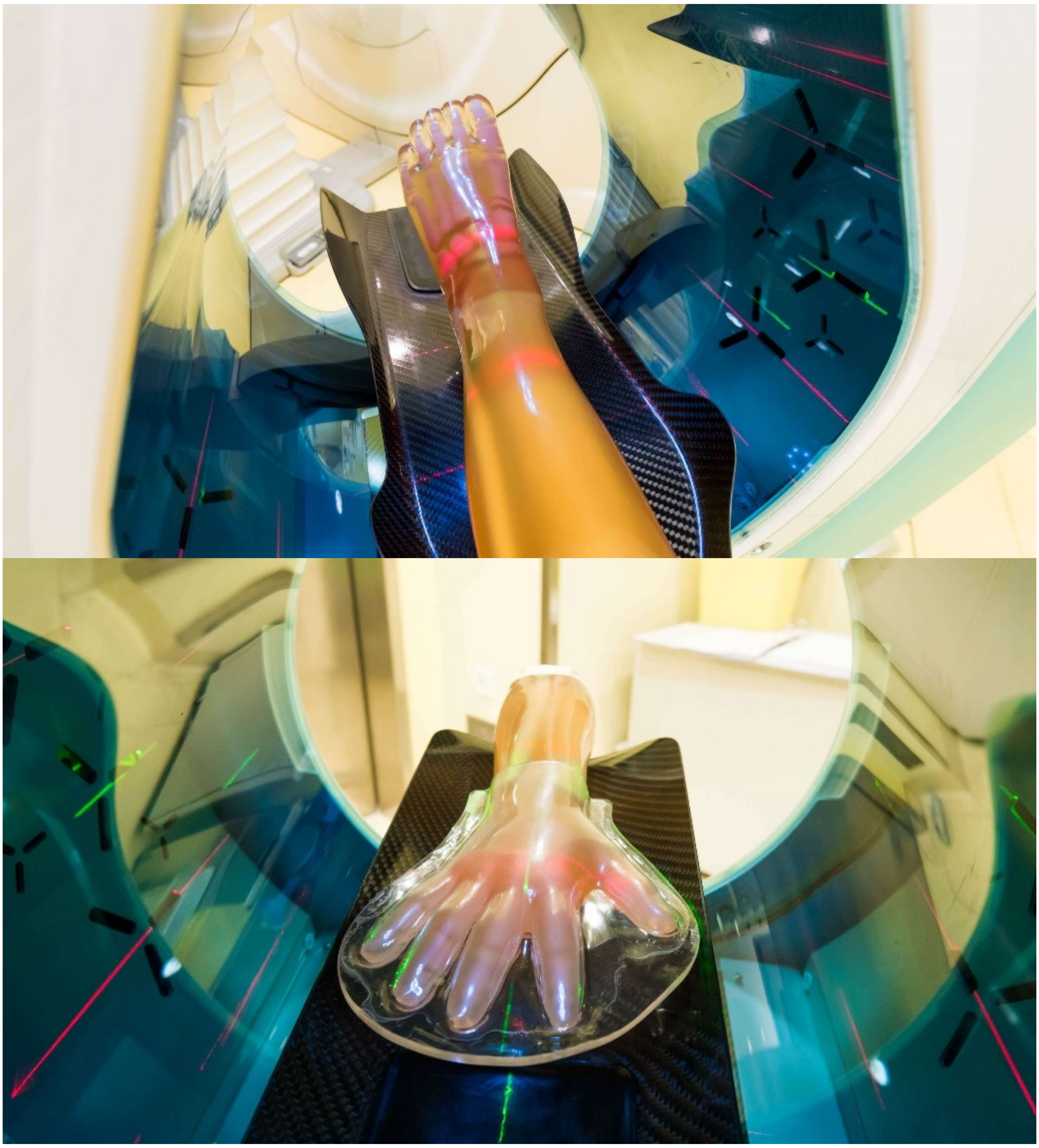

Figure 6. Ankle (above) and wrist (below) phantom in the gantry of the CBCT.

2.2.1. Dosimeters

Medical physicists used 1×6 mm square rod thermoluminescence dosimeters (TLD) made of Lithium fluoride (LiF) TLD-100™ (Thermo Fisher Scientific Inc., Waltham, Massachusetts, USA) to capture surface radiation doses. X-ray quality of CBCT and MDCT was taken into consideration individually TLDs, by applying calibration and correction factors determined by the Competence Center of Medical Physics and Radiation Protection, University Hospital of Graz, Austria. The WinREMS software analyzed the TLD glow-curves generated by a Harshaw TLD Model 5500 reader equipped with planchet heating system (Thermo Fisher Scientific Inc., Waltham, Massachusetts, USA). We measured surface doses in six positions around the examined joints, at every 1, 3, 5, 7, 9, and 11 o'clock position. In every measurement cycle, a pair of TLDs were stuck onto the phantom as depicted in Figure 7. All dosimeters were consecutively irradiated ten times per study protocol, which ensured that a sufficient amount of radiation had been applied for the readout process. Moreover, all protocols were repeated three times to prove the consistency of the measurements. After the separate exposures, an experienced medical physicist interpreted the TLD readouts. 322 (of 324) TLD readouts were conducted successfully, while 2 TLD readouts failed as a consequence of material fatigue (21).

Figure 7. TLDs attached in clockwise positions around the pediatric wrist phantom. Before the start of every measurement, we manually taped the dosimeters to the phantoms as depicted in the image above.

2.3. Patients

2.3.1. Patients receiving CBCT

From September 2015 to June 2016, we prospectively recruited a total number of 59 unique pediatric patients (32 male, 27 female), who received CBCT examinations of at least one extremity region. The mean age of the patients was 14.3 years (range 8.8 to 17.7 years). One patient underwent CBCT examinations of two different joints, and one patient had a follow-up CBCT, resulting in overall 61 performed CBCT studies. These patients were referred by the local pediatric surgeons to clinically indicated CT examinations of injured extremities. In consenting patients, CBCT examinations were performed by radiological technologists instead of the usually done MDCTs.

2.3.2. Patients undergoing MDCT

A limited subgroup of 10 patients (8 male, two female) agreed to undergo both CBCT and MDCT in parallel. We retrospectively matched the other 51 CBCTs to MDCTs from the local PACS archive manually. These had all been performed on the same study MDCT device, sex, and extremity region, and at the same age in years in the last decade. Seven of the 61 CBCT-MDCT pairs were excluded due to discrepancies in the presence of casts or metal implants. 54 study pairs remained for further comparisons (wrist n=19, ankle n=11, elbow n=9, finger n=6, foot n=5, hand n=3, knee n=1). Figure 8 details the above-described recruitment process leading to a mean patient age of 14.3 ±2.2 years in CBCT versus 14.4 ±2.2 years in MDCT; each group contained 24 females and 30 males. Age differences did not reach statistical significance (p=0.832).

2.3.3. Patients sustaining DR

Fifty-eight digital radiographs (DRs) of the same region as in CBCT were available for comparison. Of these 58 CBCT-DR pairs, eleven were excluded because of a date difference of more than 14 days. Thus, 47 CBCT-DR pairs (wrist n=16, ankle n=11, elbow n=6, finger n=5, foot n=4, hand n=4, knee n=1) were included.

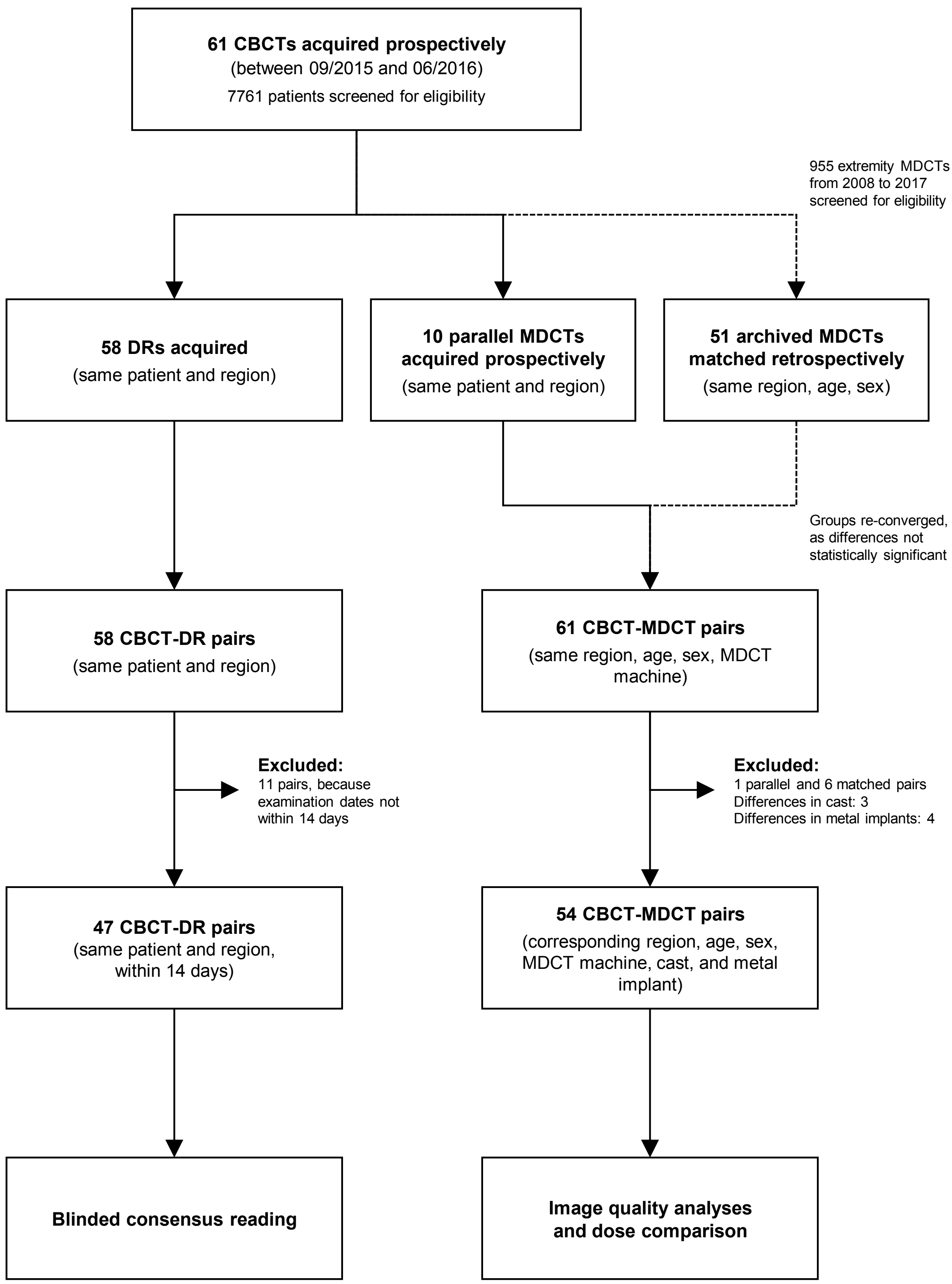

Figure 8. Flowchart of the study design. Beginning with the prospectively acquired CBCT studies, we assigned the corresponding DR and MDCT examinations for further analyses.

2.4. Image acquisition

2.4.1. Phantom scanning settings

Concerning the measurements of surface doses in the pediatric phantoms, we generated three imaging protocols called CBCT, MDCT (routine), and MDCT (CTDI equivalent). The MDCT (routine) protocol was actually in use at the author's clinical division. When considering the unalterable linkage between selected radiation dose and resulting image quality, marked differences in peak kilovoltages and tube currents, as well as different ways of image acquisition and reconstruction between the study devices, make clear that we could not perfectly match the machines for the comparison. Therefore, the pediatric radiologists at our division consensually agreed on CBCT exposure settings based on initial scans of animal limbs. In every extremity region, three age-dependent exposure levels were prepared with the goal of barely sufficient image quality to diagnose a respective fracture securely. Manufacturer's preselected parameters were labeled "high," representing a suitable option for teenagers older than 12 years. The two other exposure levels were called "medium" (suitable for schoolers aged 6 to 12 years) and "low" (preschoolers younger than six years) (21).

The MDCT protocol set named "MDCT routine" contained the routinely used MDCT exposure settings at the local institution. A second MDCT protocol denoted "MDCT (CTDI equivalent)" was matched to the dose of CBCT protocols based on the $CTDI_{vol}$ (16 cm phantom). With this protocol, we intended to demonstrate dose conformity between CBCT and MDCT. Table 1 summarizes the three protocols and their respective exposure settings for scanning the pediatric wrist and ankle phantoms (21).

Table 1. Exposure parameters for scanning phantoms of the ankle and wrist.

Protocol	Phantom	Exposure level	kVp	mA	Rotation time (sec)	mAs (effective)	$CTDI_{vol}$ (16cm phantom)	DLP (mGy*cm)
CBCT	Ankle	low	80.0	4.0	6.000	24.0	1.1	14.5
		medium	84.0	6.0	6.000	36.0	2.1	26.9
		high	92.0	8.0	6.000	48.0	4.0	51.6
	Wrist	low	80.0	2.0	6.000	12.0	0.6	7.2
		medium	84.0	4.0	6.000	24.0	1.4	18.0
		high	88.0	6.0	6.000	36.0	2.5	32.5
MDCT (routine)	Ankle	low	100.0	30.0	0.500	15.0	1.6	20.3
		medium	120.0	30.0	0.500	15.0	2.5	29.5
		high	120.0	40.0	0.500	20.0	3.2	39.4
	Wrist	low	100.0	30.0	0.500	15.0	1.4	16.7
		medium	120.0	20.0	0.500	10.0	1.6	17.6
		high	120.0	30.0	0.500	15.0	2.2	26.3
MDCT (CTDI equivalent)	Ankle	low	80.0	20.0	1.000	20.0	1.1	13.5
		medium	100.0	50.0	0.375	18.8	2.1	25.3
		high	120.0	30.0	0.750	22.5	4.0	47.8
	Wrist	low	80.0	30.0	0.375	11.3	0.6	7.7
		medium	100.0	20.0	0.625	12.5	1.4	17.4
		high	120.0	40.0	0.375	15.0	2.5	29.6

All relevant parameters (kVp, mA, mAs, and dose measures) for phantom irradiations are shown for CBCT, MDCT (routine), and MDCT (CTDI equivalent) protocols (21).

Images were reconstructed in three planes relative to the axis of the examined body part (axial, coronal and sagittal). Slice thickness was set to 1.4 mm.

2.4.2. Patient scanning settings

Typical parameters used for scanning patients prospectively with CBCT and MDCT (parallel and matched) are shown in Table 2.

Table 2. Exposure parameters and reconstruction settings of both study devices for patient scanning.

		CBCT (Planmed Verity)	MDCT (Toshiba Aquilion One)	Significant differences (p)
Image acquisition	Field of view (mm)	160 x 160	120 x 120	-
	$CTDI_{vol}$ [16 cm phantom] mGy (mean SD)	2.3 ±0.8	3.2 ±1.0 without AIDR3D 4.1 ±1.0 with AIDR3D 2.9 ±0.7	p<0.001 p<0.001 p<0.001
	DLP mGy*cm (mean ±SD)	27.9 ±11.9	34.8 ±18.1 without AIDR3D 45.4 ±21.9 with AIDR3D 30.3 ±14.3	p=0.021 p<0.001 p=0.378
	kVp (mean ±SD)	91.0 ±3.5	120.0 ±2.7	p<0.001
	mA (mean ±SD)	4.6 ±1.4	37.6 ±11.3	p<0.001
	mAs (mean ±SD)	27.6 ±8.5	19.0 ±5.8	p<0.001
	Rotation / exposure time (seconds)	6.0 / 36.0	0.5 / 0.5	p<0.001
Image reconstruction	Slice thickness (mean ±SD)	1.3 ±0.2 mm	1.3 ±0.3 mm	p=0.104
	Planes	axial, coronal, sagittal	axial, coronal, sagittal	-
	Kernel	Sharp	FC 18 [AIDR3D (after 2012)] /STD/W/CB	-
	Pixel matrix	800x800	512x512	-
	Pixel spacing (mean ±SD)	0.2 ±0.0 mm	0.2 ±0.1 mm	p=0.009

Relevant parameters are given for the CBCT and the MDCT machine.

2.5. Image analyses

We analyzed all collected imaging studies (CBCT, MDCT, and DR) semi-objectively and subjectively in a random manner and blinded to the examination details. To achieve anonymization, the doctoral candidate loaded the examinations into synedra View Personal, Version 17 “Poseidon” (synedra information technologies GmbH, Innsbruck, Austria, https://www.synedra.com/), manually assigned ID-numbers and automatically removed any kind of personal information.

2.5.1. Semi-objective image analysis

The doctoral candidate (Observer 1, S.T.), a radiology resident with six years of professional experience, performed all semi-objective image analyses by opening and arranging a pair of CBCT and MDCT examinations side by side in FIJI 1.49v (133) an ImageJ distribution (open source image processing software, http://rsbweb.nih.gov/ij/). The investigator placed polygonal regions of interest (ROI) in corresponding axial image slices, which was repeated three times in different matching slice positions for every structure. The arithmetically averaged mean and standard deviation of the readout Hounsfield units (HU) or, respectively grey values for cortical bone, fat, muscle, and the background air was noted. We also generated a logarithmic histogram of every whole axial image stack’s grey values, to retrieve the spectrum of grey values including the minimum and maximum pixel intensity, and to manually locate the upper boundary of the cortical bone peak. Both parameters were necessary to normalize the examinations, as deficient comparability between the device’s HU is known (134-138).

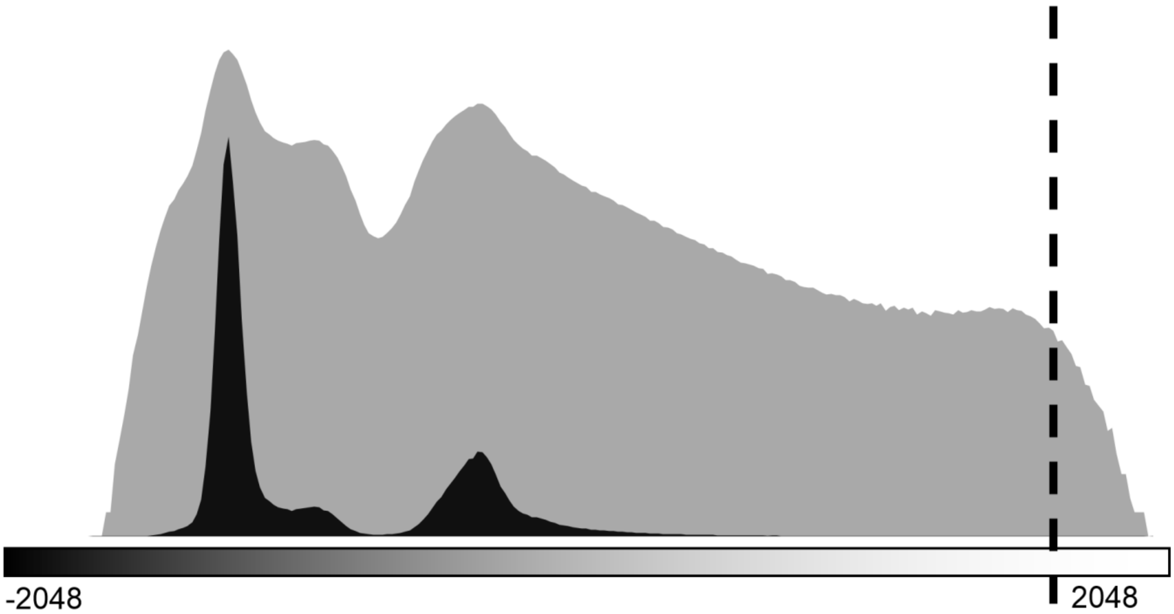

Figure 9. Histogram of a sample axial CT stack. Data is presented in absolute values (black area) and logarithmic transformation (the grey area). The peak of cortical bone was manually selected based on the logarithmic histogram. The histogram was generated with ImageJ.

In ankle and wrist phantoms, normalized/corrected image noise, contrast-to-noise and signal-to-noise ratios (CNR and SNR respectively) were calculated based on the before-mentioned parameters. Image noise was defined as the mean standard deviation of air, and was corrected by dividing it through the mean thousandth HU of cortical bone as the densest structure (NOISE = SD air / [MEAN cortical bone * 0.001]). CNR was calculated by subtracting mean air from mean cortical bone and dividing it through the standard deviation of air (CNR = [MEAN cortical bone – MEAN air] / SD air). SNRs were calculated for all tissues separately by dividing mean tissues by their respective standard deviations (SNR = MEAN tissue / SD tissue) (21).

In the ten examinations that were performed parallel in traumatized patients, a correction factor for the cortical bone was calculated from the differences in the cortical bone peaks, shown in Figure 9. Hounsfield units in MDCT were 37% higher than the grey values in CBCT examinations, which was considered and corrected in CBCT studies (HU_{corr}).

2.5.2. Subjective image impression

Three pediatric radiologists with 4, 6 and 28 years of experience in reporting musculoskeletal CT rated subjective image quality consensually on a Likert scale with five grades (1 = excellent, 2 = good, 3 = average, 4 = fair, 5 = poor). The analyzed features were overall image quality, sharpness, noise, contrast, beam hardening, ring, and aliasing artifacts (21).

Two observers, pediatric radiologists with at least three years of experience in interpreting musculoskeletal CT studies (Observer 1 = S.T. and Observer 2 = R.M.), analyzed all anonymized examinations. We randomly assigned ID numbers to all studies. After image analysis, a questionnaire on subjective image impression was filled out. The observers rated diagnostic certainty, image quality and artifacts as displayed in Table 2. Radiologists reviewed the studies in a dark reading room on calibrated four-megapixel RadiForce RX440 monitors (Eizo, Hakusan, Japan), and presented the images in the local PACS software syngo.plaza VB20A (Siemens Healthineers, Erlangen, Germany). The observers assessed the studies in bone and soft tissue windows and were allowed and encouraged to alter center and windows settings as desired.

2.5.3. Comparison of CBCT and DR

In consensus, the doctoral candidate (S.T.) and a radiologist with 29 years of professional experience (E.S.) established a reference reading of the 47 study pairs. This evaluation considered all available information, clinically (information in the local hospital information system, including follow-up visits) as well as radiologically (DR, CBCT, MDCT, MRI) to decide, whether a recent fracture was present.

Two radiologists with 4 (E.N.) and 8 (R.M.) years of experience in musculoskeletal imaging rated DR and CBCT studies blinded and randomly on professional equipment with a delay of at least four weeks between the modalities. The parameters of interest were the presence of a recent fracture, the diagnostic certainty, and the image quality.

2.6. Statistical analyses

Collected data were imported and processed in SPSS Statistics Version 21 (IBM Corp., Armonk, NY). Descriptive tests were used to explore the obtained values. In the case of a proven normal distribution, mean values were compared with independent samples t-tests. Median and ranges are given for parameters lacking a normal distribution, followed by non-parametric testing. Pearson linear correlations were calculated to show relations between radiation dose and image quality. We used intraclass correlation coefficients [two-way mixed average measures, ICC(3,k)] to demonstrate test-retest reliability, and also prepared a Bland-Altman plot. The blinded CBCT and DR readings were compared with the reference test by calculating the area under the curve (AUC), sensitivity and specificity. The nonparametric Wilcoxon signed-rank test evaluated diagnostic certainty. As a general rule, p values lower than 0.05 were assumed to be statistically significant.

2.7. Ethics committee

Local ethics committee (Medical University of Graz, IRB00002556) approval was obtained (No. 27-452 ex 14/15) before the prospective CBCT examinations. Patients and parents were educated about study-related chances and risks and needed to give written informed consent before undergoing CBCT image acquisitions. An additional ethics committee vote was granted for retrospective MDCT(-CBCT) study matchings (No. 30-508 ex 17/18). Phantom dose measurements did not require an ethical review board authorization.

3. Results

Analyses from surface dose measurements performed in phantoms of the pediatric ankle and wrist as well as patient scans of CBCT compared with MDCT are presented in the following sections.

3.1. Phantom surface dose assessment

Mean surface radiation dose equaled 3.0 ±1.9 mGy in CBCT (average of the low, medium, and high protocols for ankle and wrist). The surface doses were significantly higher in the MDCT (routine) protocol ($p<0.001$), with 3.9 ±1.1 mGy. As presumed, we saw no statistically significant difference between CBCT and the CTDI-equivalent MDCT protocol, with a mean of 3.0 ±1.9 mGy, and 3.0 ±1.4 mGy respectively ($p=0.903$) (21).

Surface doses significantly correlated linearly with $CTDI_{vol}$ ($R=0.957$) and DLP (0.950), both $p<0.001$, and were found to be significantly lower compared to MDCT (routine) apart from the “high” exposure setting in the ankle and the wrist phantom ($p=0.633$) and the “high” ($p=0.131$) as well as overall three settings in the ankle phantom ($p=0.053$) (21). Table 3 summarizes the particular findings.

Table 3. Results of surface dose measurements between CBCT and MDCT (routine).

Phantom	Exposure level	Protocol	Valid pairs (n)	Mean (mGy)	SD (mGy)	Significance (p)
Ankle + Wrist	low + medium + high	CBCT	107	3.0	1.9	<0.001
		MDCT (routine)	108	3.9	1.2	
Ankle	low + medium + high	CBCT	53	3.8	2.1	0.053 ns
		MDCT (routine)	54	4.5	1.3	
Wrist	low + medium + high	CBCT	54	2.2	1.3	<0.001
		MDCT (routine)	54	3.4	0.7	
Ankle + Wrist	low	CBCT	36	1.3	0.5	<0.001
		MDCT (routine)	36	3.0	0.3	
	medium	CBCT	36	2.8	0.9	<0.001
		MDCT (routine)	36	3.7	0.8	
	high	CBCT	35	5.0	1.7	0.633 ns
		MDCT (routine)	36	5.1	0.9	
Ankle	low	CBCT	18	1.8	0.4	<0.001
		MDCT (routine)	18	3.0	0.4	
	medium	CBCT	18	3.4	0.8	<0.001
		MDCT (routine)	18	4.5	0.4	
	high	CBCT	17	6.4	1.2	0.131 ns
		MDCT (routine)	18	5.9	0.6	
Wrist	low	CBCT	18	0.9	0.2	<0.001
		MDCT (routine)	18	2.9	0.3	
	medium	CBCT	18	2.1	0.3	<0.001
		MDCT (routine)	18	3.0	0.3	
	high	CBCT	18	3.6	0.9	0.004
		MDCT (routine)	18	4.4	0.4	

Summary of the results including independent samples t-test for CBCT and MDCT (routine) in both phantoms. All three exposure settings are displayed. The letters "ns" indicate non-significant differences (21).

Caused by the incomplete tube rotation (210 degrees) of the CBCT device, TLDs at the posterior 5 and 7 o'clock locations received significantly less surface dose when compared to their anterior counterparts at 1 and 11 o'clock, with an average of 2.5 ±1.5 mGy and 3.5 ±2.0 mGy respectively (p=0.014). This finding is graphically demonstrated in Figure 10. The MDCT TLDs did not show this behavior, as tube rotation is here complete with 360 degrees (21).

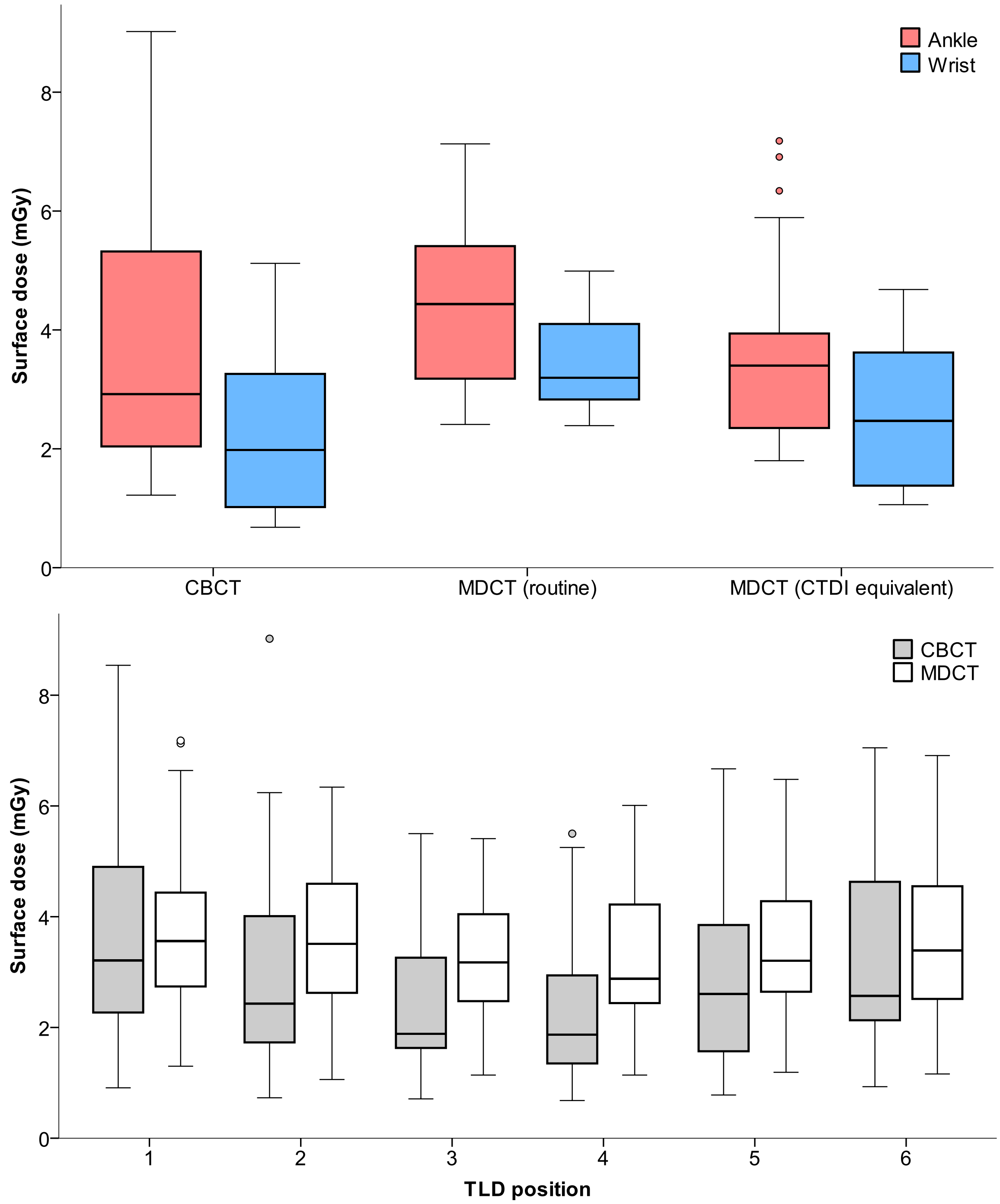

Figure 10. Box plots of surface radiation doses. On top: Mean surface radiation doses of the three exposure protocols in the ankle and wrist phantoms. At the bottom: Doses of the different TLD positions in the pediatric ankle and wrist phantoms (21).

Table 4. Collected dose measurements (mGy) displayed for both devices, both phantoms, and all used protocol settings (21).

Protocol	Phantom	Exposure level	TLD 1 mean (mGy)	TLD 2 mean (mGy)	TLD 3 mean (mGy)	TLD 4 mean (mGy)	TLD 5 mean (mGy)	TLD 6 mean (mGy)	Total TLD mean (mGy)	Total TLD SD (mGy)
CBCT	Ankle	low	2.2	1.7	1.6	1.4	1.6	2.1	**1.8**	**0.4**
		medium	4.3	3.4	2.6	2.7	3.1	4.3	**3.4**	**0.8**
		high	7.7	7.1	5.3	5.3	6.2	7.0	**6.4**	**1.2**
	Wrist	low	1.0	0.9	0.8	0.7	0.8	1.1	**0.9**	**0.2**
		medium	2.6	2.0	1.8	1.7	2.2	2.4	**2.1**	**0.3**
		high	4.4	3.7	2.8	2.8	3.9	4.3	**3.6**	**0.9**
MDCT (routine)	Ankle	low	3.2	3.3	2.9	2.7	2.9	3.0	**3.0**	**0.4**
		medium	4.3	4.5	4.3	4.3	4.4	4.9	**4.5**	**0.4**
		high	6.6	5.5	5.2	5.5	6.1	6.3	**5.9**	**0.6**
	Wrist	low	3.3	2.8	2.6	2.7	3.0	3.1	**2.9**	**0.3**
		medium	3.1	3.3	3.1	2.7	2.8	3.0	**3.0**	**0.3**
		high	4.6	4.7	4.3	4.2	4.3	4.1	**4.4**	**0.3**
MDCT (CTDI equivalent)	Ankle	low	2.4	2.4	2.0	1.8	2.1	2.3	**2.2**	**0.3**
		medium	3.4	3.5	3.2	3.0	3.3	3.7	**3.4**	**0.4**
		high	5.6	5.3	4.5	4.6	5.1	6.4	**5.2**	**1.1**
	Wrist	low	1.4	1.3	1.3	1.2	1.2	1.3	**1.3**	**0.1**
		medium	2.6	2.4	2.3	2.2	2.5	2.4	**2.4**	**0.2**
		high	4.1	3.9	3.7	3.8	3.9	4.0	**3.9**	**0.4**

In the phantoms, all semi-objective image quality parameters were superior in CBCT ($p<0.001$), despite activated iterative reconstruction in MDCT. Average noise was 33.3 ±17.8 HU_{corr} in CBCT, and 63.2 ±15.6 HU in MDCT. Corrected CNR was 55.4 ±28.5 HU_{corr} in CBCT, and 39.4 ±5.1 HU in MDCT. Corrected SNR was 28.2 ±15.1 HU_{corr} for CBCT, and 8.8 ±1.8 HU for the MDCT machine (21).

Correlation analyses revealed that overall the subjective image quality decreased, the lower the exposure settings were chosen (0.594, $p=0.009$). In that context, surface doses significantly negatively correlated with image quality (CBCT R=-

0.816, p=0.048; MDCT R=-0.693, p=0.012). On average, total image quality did not differ significantly (p=0.456) between CBCT (2.7 ±0.8 points) and MDCT (3.0 ±1.0 points), as well as between the study protocols [2.7 ±0.8 points for CBCT, and 2.3 ±0.5 points for MDCT (routine), p=0.421]. Moreover, sharpness and contrast were not different too (21).

We found a significant linear correlation between semi-objective (measured) and subjective (rated) noise assessments (R=0.809, p<0.001). The raters found more beam hardening artifacts in CBCT, and more noise and aliasing in MDCT (p<0.001) (21). Detailed median subjective image quality ratings are given in Table 5.

Table 5. A consensus rating of image quality in the pediatric ankle and wrist phantoms.

Protocol	**Phantom**	**Exposure level**	**Overall quality**	**Contrast**	**Sharpness**	**Noise**	**Beam hardening**	**Aliasing**
CBCT	Ankle	low	3	1	3	2	3	2
		medium	2	2	2	2	3	1
		high	2	2	1	1	2	1
	Wrist	low	4	3	4	2	4	2
		medium	3	1	2	1	3	2
		high	2	1	1	1	3	2
MDCT (routine)	Ankle	low	3	1	3	4	1	4
		medium	2	2	3	3	1	3
		high	2	2	2	2	1	3
	Wrist	low	3	1	2	4	1	3
		medium	2	1	3	2	1	3
		high	2	1	2	3	1	4
MDCT (CTDI equivalent)	Ankle	low	4	1	4	5	1	4
		medium	4	2	4	4	1	3
		high	3	3	3	3	1	3
	Wrist	low	5	1	5	5	1	3
		medium	3	2	4	3	1	3
		high	3	2	3	3	1	3

The table lists all study protocols and exposure settings, ranging from 1 = excellent to 5 = poor on a five-point Likert scale (21).

With a total ICC(3,k) of 0.953, an excellent test-retest reliability was found for the TLD surface dose assessments (p<0.001). Divided into CBCT and MDCT, ICCs were 0.946 and 0.922 (both p<0.001) respectively (21). The results of the test-retest reliability are demonstrated in Figure 11.

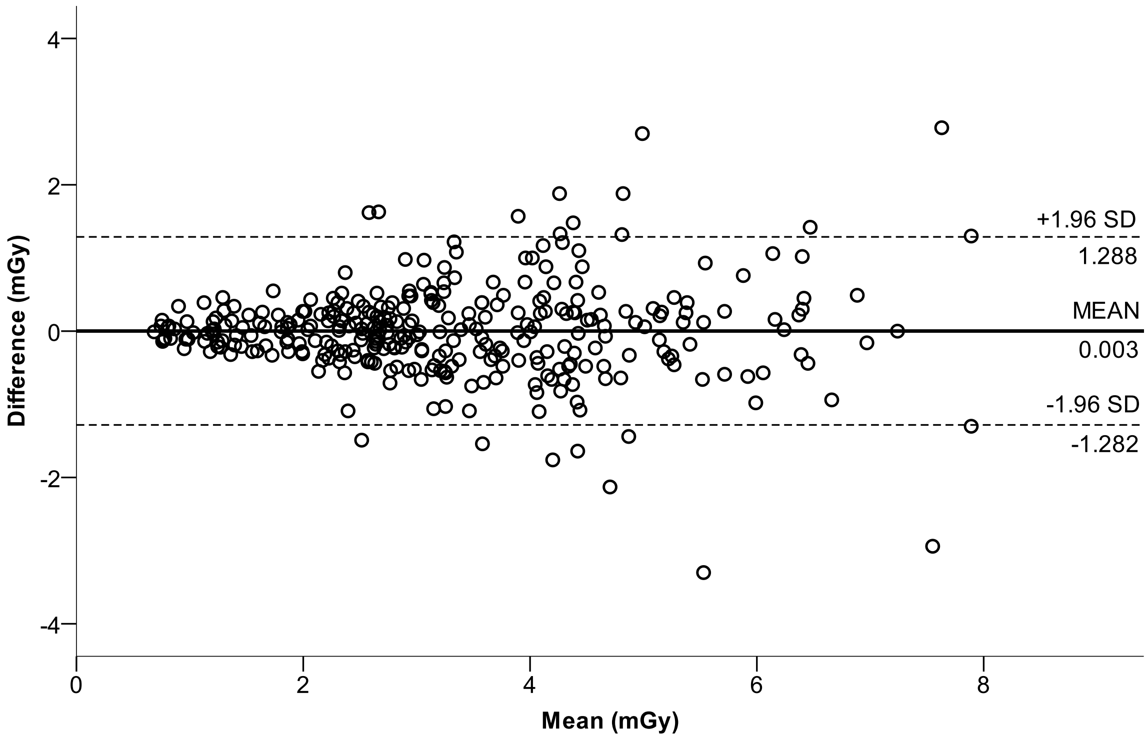

Figure 11. A Bland-Altman plot depicts test-retest reliability of the conducted surface dose analyses in the pediatric ankle and wrist phantoms. The drawn through horizontal line represents the mean value of 0.003 (SD ±0.66) mGy. The dotted horizontal lines are the upper and lower 1.96 SD intervals at 1.288 and -1.282 mGy. The plot includes valid measurements from all six TLD positions (21).

3.2. Comparison of CBCT and DR

The reference reading procedure of the 47 compared CBCT-DR pairs defined 26 (55.3%) studies with and 21 (44.7%) without the presence of a recent visible fracture.

Blinded Observer 1 had an AUC of 0.938 (sensitivity 0.923, specificity 0.952) for diagnosing a fracture in CBCT, and 0.779 (sensitivity 0.654, specificity 0.905) in DR. Observer 2's AUC was 0.918 (sensitivity 0.885, specificity 0.952) in CBCT, and 0.708 (sensitivity 0.654, specificity 0.762) in DR. One scaphoid fracture was not diagnosed by both observers, only clearly visible on a supplementing MRI examination.

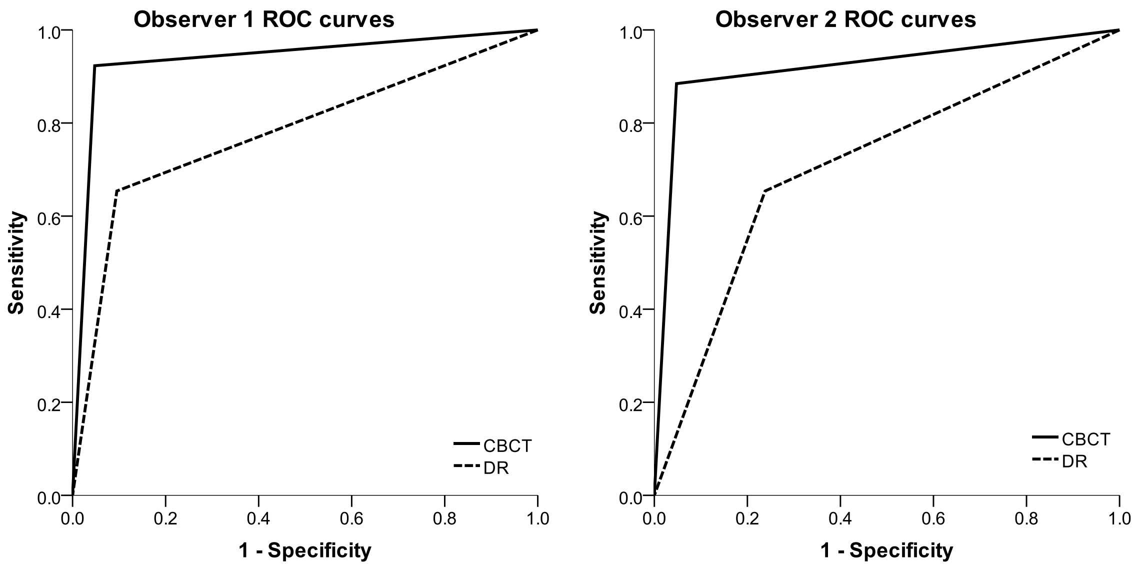

Figure 12. ROC curves of both observers for CBCT and DR.

Observer 1 rated diagnostic certainty significantly higher in CBCT than DR ($p=0.011$) using the Wilcoxon signed-rank test, whereas Observer 2 did not ($p=0.156$).

3.3. Comparison of CBCT and MDCT

The performed non-parametric tests revealed no statistically significant differences regarding MDCTs performed in parallel and MDCTs matched retrospectively in the main image quality parameters [noise $p=0.250$, CNR $p=0.880$, SNR (bone $p=0.825$, fat $p=0.250$, muscle $p=0.280$), CT dose index ($CTDI_{vol}$) $p=0.269$, and Dose length product (DLP) $p=0.478$]. Both MDCT groups were therefore recombined and treated as a single entity in the further analyses.

Corrected image noise was on average significantly lower in CBCT, compared to MDCT with 28.4 HU_{corr}, and 52.2 HU ($p<0.001$). So was mean normalized CNR with 112.1 ±26.6 HU_{corr} in CBCT and MDCT 59.3 ±13.5 HU ($p<0.001$).

Normalized SNRs were found to be significantly different for cortical bone (CBCT = 2054 ±303 HU_{corr} and MDCT = 1955 ±173 HU, $p<0.001$), fat (CBCT = 39 ±8 HU_{corr}

and MDCT = 21 ±4 HU, p<0.001), and muscle (CBCT = 38 ±8 HU_{corr} and MDCT = 22 ±4 HU, p<0.001). The mentioned values are shown in Figure 13.

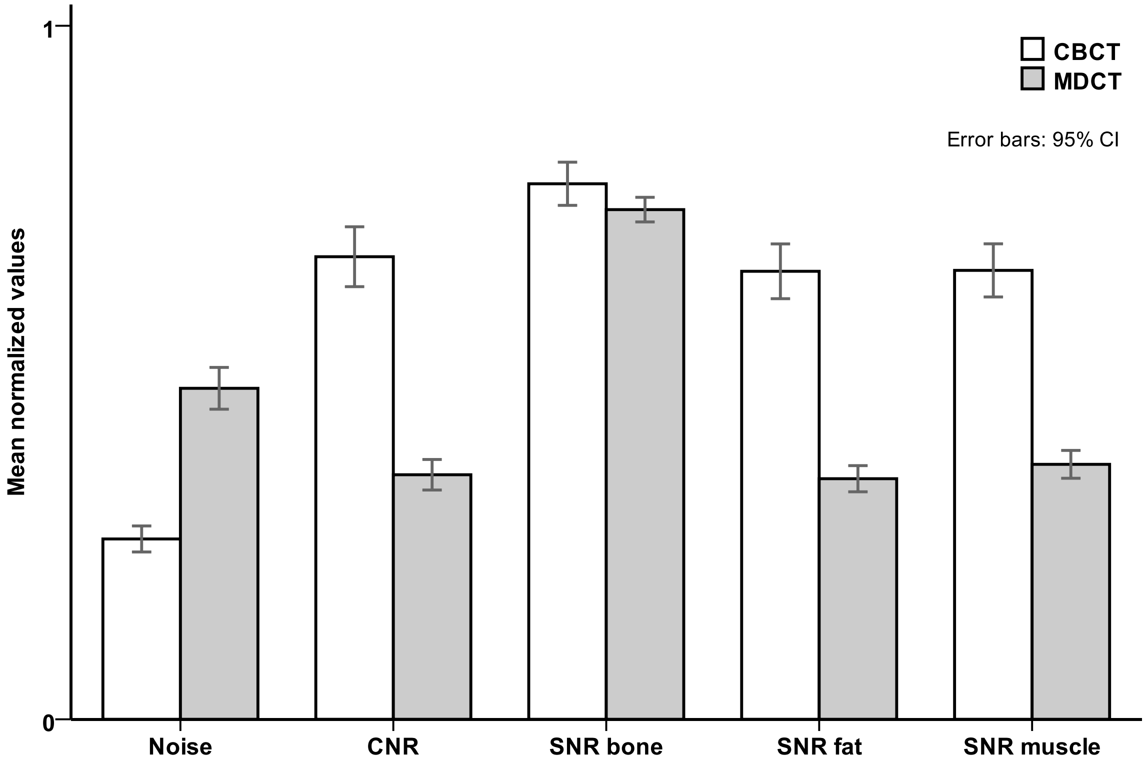

Figure 13. Semi-objective image quality parameters compared between CBCT and MDCT, presented as a bar-chart. 95% confidence interval (CI) error bars are displayed.

Subjective image quality comparison revealed a median overall image quality rating of 3 (range 2 to 5 points) in CBCT and 2 in MDCT (range 1 to 4 points), statistically significantly different (p<0.001). Diagnostic certainty was also rated in favor of MDCT (CBCT = 1, range 1 to 5, and MDCT = 1, range 1 to 2 points, p<0.001). Image sharpness, the depiction of fine details and visualization of trabecular bone were rated significantly better in CBCT, while image contrast and joint representation were superior in MDCT. Cortical bone and soft tissue were not significantly different in the conducted observer grading in the available soft tissue kernels.

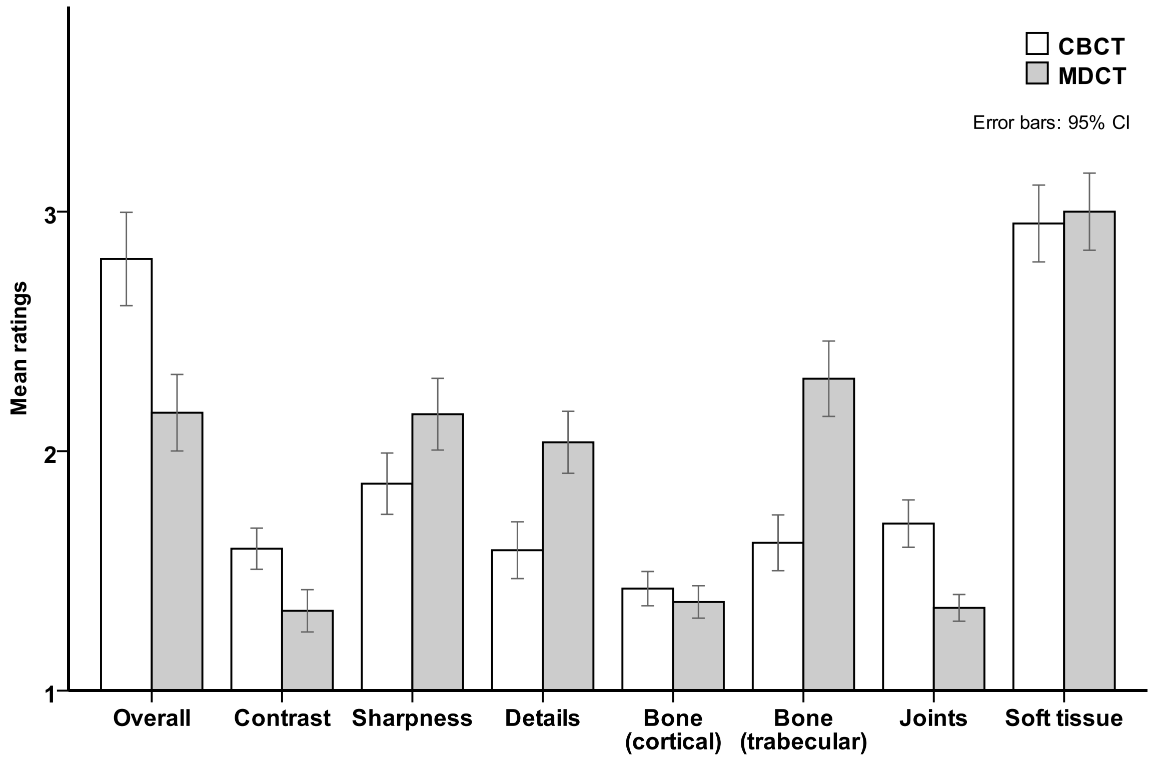

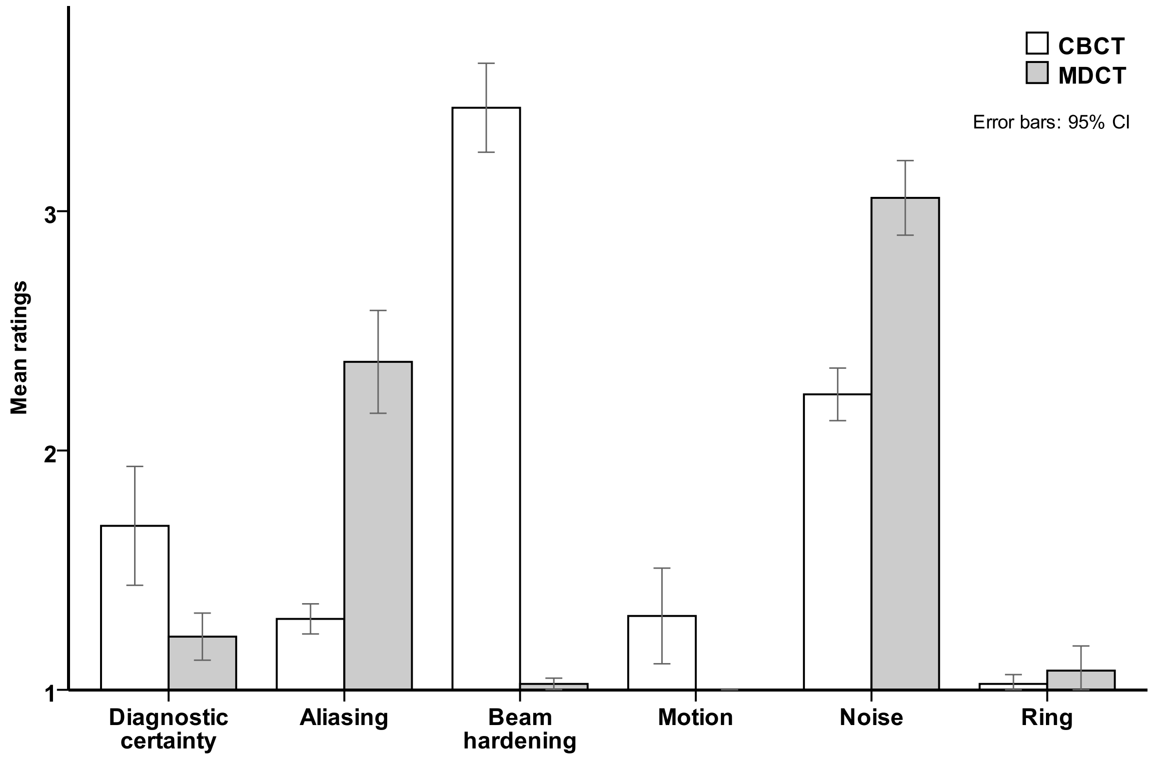

Figure 14. Subjective image impression ratings. Top) Mean image quality and artifacts, independently rated by three pediatric radiologists. Bottom) Diagnostic certainty ratings and image artifacts.

Concerning artifacts, the observers rated beam hardening more severely in CBCT (median 3, range 2 to 5 points in CBCT; and median 1, range 1 to 1 point in

MDCT; $p<0.001$). Noise was less pronounced in CBCT (median rating 2, range 1 to 3 in CBCT; and 3, range 2 to 5 points in MDCT; $p<0.001$), as was aliasing (median 1, range 1 to 2 points in CBCT; and 2, range 1 to 5 points in MDCT, $p<0.001$). Ring artifacts were uncommon, without statistically significant differences. Motion artifacts were rarely, but exclusively seen in CBCT (median 1, range 1 to 5 points in CBCT; and 1, range 1 to 1 point in MDCT, $p=0.013$).

Semi-objective image noise measurements and subjective noise ratings correlated significantly ($R=0.631$, $p<0.001$). Contrast perception and CNR were associated ($R=0.222$, $p=0.021$). A negative correlation was seen between pixel-spacing and sharpness impression ($R=-0.231$, $p=0.016$).

Table 6. Subjective image interpretation.

				Group differences (Median tests) between CBCT and MDCT					Interrater differences [ICC(3,k)] separate for CBCT and MDCT			
Category	**Parameter**	**Possible answers**	**Modality**	**Median (Mean*) [parallel/matched]**	**Range (SD*) [parallel/matched]**	**Min [parallel/matched]**	**Max [parallel/matched]**	**Significance (p)**	**ICC**	**95% CI (lower limit)**	**95% CI (upper limit)**	**Significance (p)**
General	Fracture	Yes or no	CBCT	0.65*	0.48*	0	1	p=0.176	0.83	0.74	0.90	p<0.001
			MDCT	0.76*	0.39*	0	1		0.88	0.80	0.92	p<0.001
	Diagnostic certainty	(Very good) 1 – 5 (Very poor)	CBCT	1	4	1	5	p<0.001	0.73	0.58	0.84	p<0.001
			MDCT	1 [1/1]	1 [0/1]	1 [1/1]	2 [1/2]		0.40	0.06	0.63	p=0.012
Image quality	Overall image quality	(Very good) 1 – 5 (Very poor)	CBCT	3	3	2	5	p<0.001	0.67	0.29	0.83	p<0.001
			MDCT	2 [2/2]	3 [2/3]	1 [1/1]	4 [3/4]		0.66	0.42	0.81	p<0.001
	Sharpness	(Very good) 1 – 5 (Very poor)	CBCT	2	2	1	3	p=0.013	0.43	0.10	0.65	p<0.001
			MDCT	2 [2/2]	2 [2/2]	1 [1/1]	3 [3/3]		0.39	-0.02	0.65	p<0.001
	Contrast	(Very good) 1 – 5 (Very poor)	CBCT	2	1	1	2	p<0.001	0.17	-0.09	0.41	p=0.063
			MDCT	1 [1/1]	1 [1/2]	1 [1/1]	3 [2/3]		0.63	0.35	0.78	p<0.001
	Detail resolution	(Very good) 1 – 5 (Very poor)	CBCT	1	2	1	3	p=0.005	0.20	-0.19	0.48	p=0.138
			MDCT	2 [2/2]	2 [2/2]	1 [1/1]	3 [3/3]		0.36	0.04	0.59	p=0.014
	Bone (cortical)	(Very good) 1 – 5 (Very poor)	CBCT	1	2	1	3	p=0.316	0.08	-0.13	0.30	p=0.209
			MDCT	1 [1/1]	1 [0/1]	1 [1/1]	2 [1/2]		0.12	-0.14	0.36	p=0.164
	Bone (trabecular)	(Very good) 1 – 5 (Very poor)	CBCT	2	2	1	3	p<0.001	0.39	0.07	0.62	p=0.001
			MDCT	2 [2/2]	3 [2/3]	1 [1/1]	4 [3/4]		0.53	0.28	0.71	p<0.001
	Joints	(Very good) 1 – 5 (Very poor)	CBCT	1	3	1	4	p=0.143	0.09	-0.08	0.28	p=0.096
			MDCT	1 [1/1]	1 [1/1]	1 [1/1]	2 [2/2]		0.08	-0.10	0.27	p=0.168
	Soft tissue	(Very good) 1 – 5 (Very poor)	CBCT	3	3	2	5	p=0.187	0.24	-0.07	0.50	p<0.001
			MDCT	3 [3/3]	2 [2/2]	2 [2/2]	4 [4/4]		0.23	-0.07	0.49	p<0.001
Artifacts	Aliasing	(None) 1 – 5 (Severe)	CBCT	1	1	1	2	p<0.001	0.01	-0.20	0.24	p=0.452
			MDCT	2 [2/2]	4 [2/4]	1 [1/1]	5 [3/5]		0.56	0.07	0.78	p<0.001
	Beam hardening	(None) 1 – 5 (Severe)	CBCT	3	3	2	5	p<0.001	0.51	0.06	0.74	p<0.001
			MDCT	1 [1/1]	0 [0/0]	1 [1/1]	1 [1/1]		-0.08	-0.89	0.38	p=0.610
	Motion	(None) 1 – 5 (Severe)	CBCT	1	4	1	5	p=0.013	0.90	0.84	0.94	p<0.001
			MDCT	1 [1/1]	0 [0/0]	1 [1/1]	1 [1/1]		-	-	-	-
	Noise	(None) 1 – 5 (Severe)	CBCT	2	2	1	3	p<0.001	0.29	-0.04	0.54	p=0.035
			MDCT	3 [3/3]	3 [2/3]	2 [2/2]	5 [4/5]		0.54	0.29	0.72	p<0.001
	Ring	(None) 1 – 5 (Severe)	CBCT	1	0	1	1	p=0.495	-0.02	-0.78	0.41	p=0.533
			MDCT	1 [1/1]	2 [1/2]	1 [1/1]	3 [2/3]		0.88	0.82	0.93	p<0.001

*Questions were answered by the observers anonymized and randomized. Differences between CBCT and MDCT and interrater correlation coefficients are given within the modalities. *Mean and SD instead of Median and Range.*

The interrater assessment showed variable agreements, with satisfying results in fracture detection, diagnostic certainty, overall image quality, and motion and ring artifacts, all listed in Table 6. All other ratings presented divisive amounts of consensus.

$CTDI_{vol}$ (16 cm phantom) was 2.3 ±0.8 mGy on average in CBCT, and 3.2 ±1.0 mGy in MDCT ($p<0.001$). DLP was 27.9 ±11.9 mGy*cm in CBCT and 34.8 ±18.1 mGy*cm in MDCT ($p=0.021$). The MDCT machine used in this study received a software update in 2012 with iterative reconstruction methods (AIDR3D) which resulted in a significant reduction of $CTDI_{vol}$ (from mean 4.1 ±1.0 mGy to 2.9 ±0.7 mGy, $p<0.001$), and DLP (from mean 45.4 ±21.9 mGy*cm to 30.3 ±14.3 mGy*cm, $p=0.004$) at approximately constant image quality parameters. When leaving the 16 MDCT examinations without AIDR3D unconsidered, $CTDI_{vol}$ was still lower ($p<0.001$), but DLP was not ($p=0.378$).

4. Discussion

Based on the conducted surface dose measurements and image quality analyses in phantoms and a small patient sample, CBCT has matured to a workable pediatric extremity CT alternative. However, there is potential for improvement compared to MDCT that tarnishes the overall performance of the modality, especially regarding beam hardening artifacts and motion artifacts. These downsides are likely to impair, if not prevent the widespread employment of CBCT in pediatric radiology at present, even more, because MDCT equipment is mandatory available and more universally employable. A user would, therefore, want a specialized device to surpass the established methods in its field of application markedly. The unique features of the examined CBCT device like mobility and weight-bearing examinations cannot wholly compensate these shortcomings, mainly when using the methods in a hospital setting. However, in case of further improvements to the CBCT disadvantages, there may be certain potential use cases.

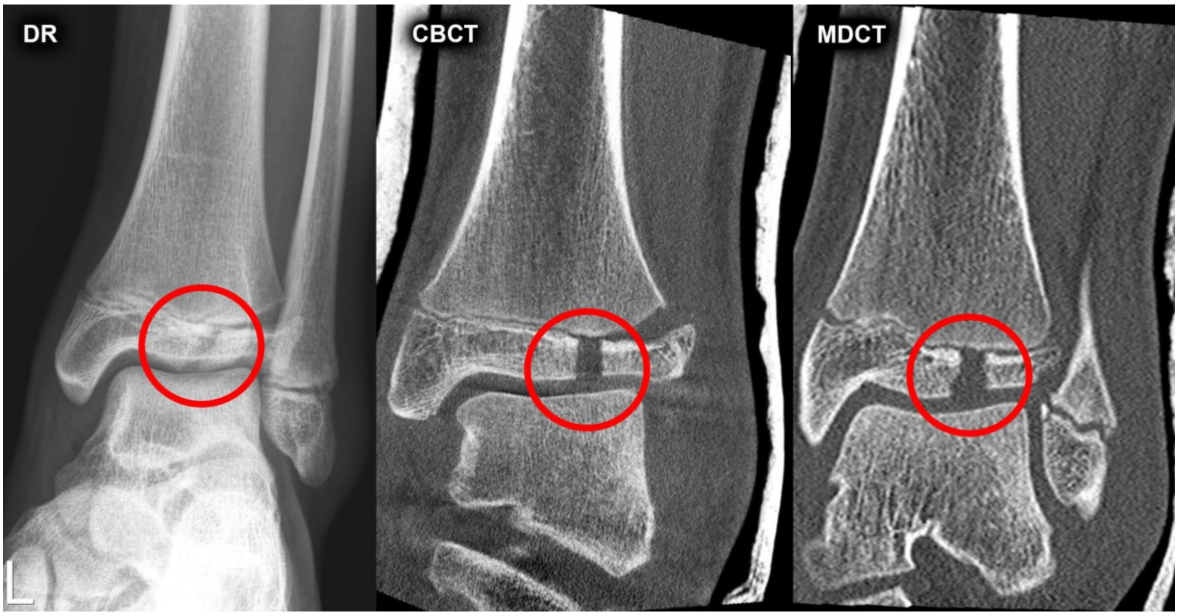

Figure 15. Example of a Tillaux fracture of the distal left tibia in an anteroposterior DR of the ankle (left), in a coronal reformat of the CBCT (middle), and MDCT (right).

4.1. Related literature

4.1.1. Comparable studies

Only one study by Pugmire et al. addressed extremity CBCT applications in children to date. The authors analyzed 34 CBCTs of the foot and ankle in children and reported that the novel method may be “a viable lower dose alternative to MDCT” and can give relevant clinical information to influence decision making possibly (20). They reported a dose saving of 43% in comparison to MDCT. As typical in studies involving children, and partly alike this manuscript, the paper suffers from a low number of included patients and the retrospective study design.

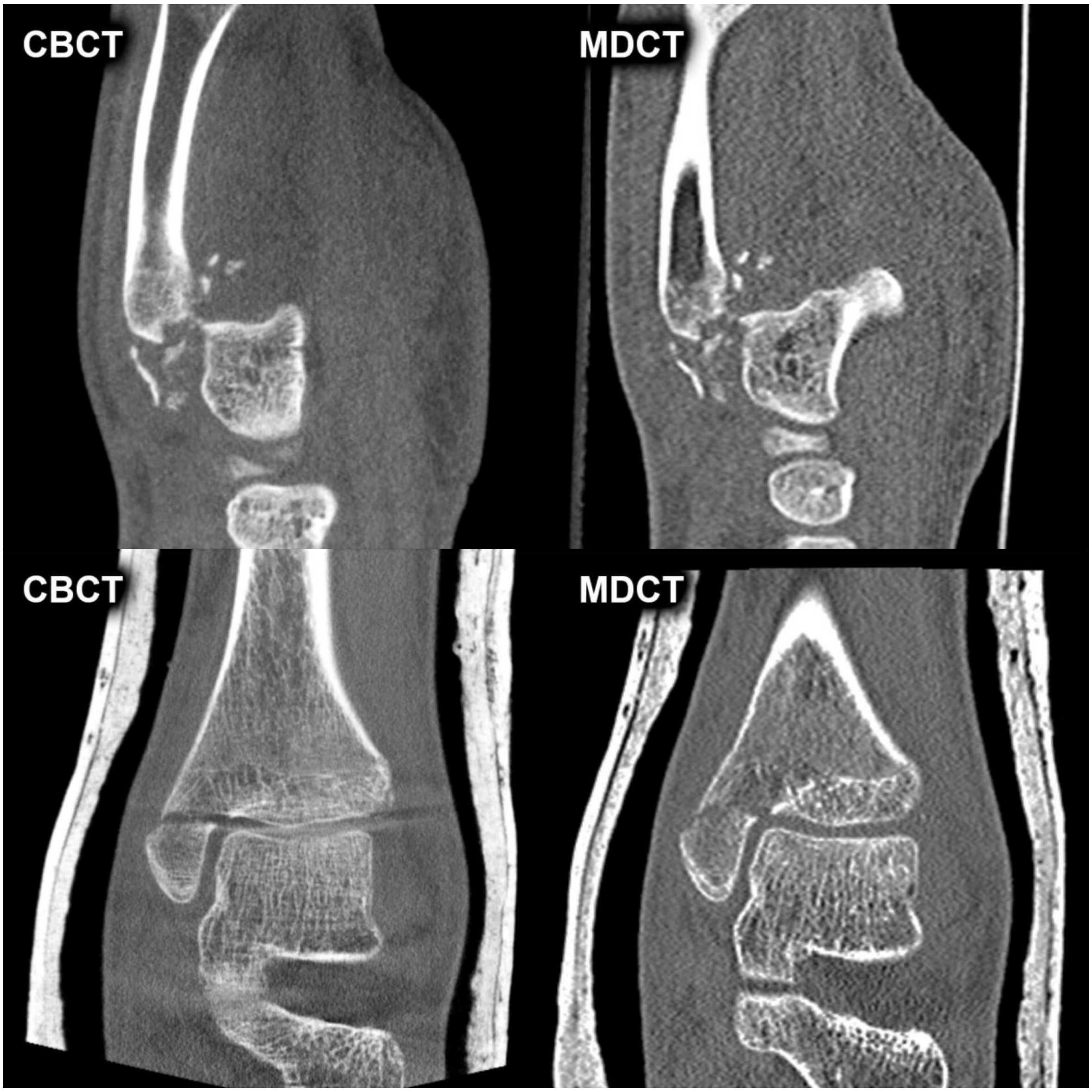

Figure 16. Side-by-side samples of CBCT and MDCT of corresponding patients. In the first row, a comminuted fracture of a metacarpal base with multiple adjacent bone fragments is seen. The second row shows a medial malleolar fracture.

4.1.2. Related studies in adults and phantoms

In adults, a few more extremity CBCT studies are available, all published in the last years.

A study by Neubauer et al. compared examinations of the hand, describing lower doses in CBCT when scanning with standard protocols (139). However, when exposure protocols were optimized in MDCT, it was able to achieve a superior image quality at lower doses than CBCT. The authors concluded that dose optimizations were useful in both modalities. A similar manuscript from the same group, by Lang et al., dealing with distal radius fractures, found that diagnostic accuracy was at a comparable level, but the depiction of the majority of anatomical structures was better in MDCT (140). The reason for this conclusion was the higher number of artifacts in CBCT, which is in accordance with the findings of our analyses in children.

Most authors described extremity CBCT as a possible alternative to MDCT (20, 127, 140, 141). Huang et al. reported their experience in 50 subjects, focusing on study durations and radiation dose. They found that CBCTs provided more relevant information than DR and occasionally MDCT, but the detection of hardware-related complications was easier in DR (142). Regarding DR, Edlund et al. described CBCT to be superior to radiography in the setting of suspected scaphoid fractures, while they diagnosed even more fractures with MRI (141). Other manuscripts assessed the diagnostic accuracy of digital radiographs compared to corresponding CBCTs in fractures of the wrist and scaphoid (143, 144). The authors reported significantly higher precision and more confidence regarding fracture detection in CBCT as a cross-sectional method, which is neither new nor surprising to anyone acquainted with medical imaging. Many studies addressed the diagnostic performance of CT compared to radiography in the setting of trauma and various regions of the human body before (145-152), and it is a well-known fact that CT outperforms X-ray examinations in many aspects. In the current work there was also one patient with a questionable scaphoid fracture in CBCT, only securely identified with MRI. Another paper by Shih et al. found CBCT to be superior than DR in recognizing subtle osteolytic changes in patients suffering from diabetic infections of the foot (153).

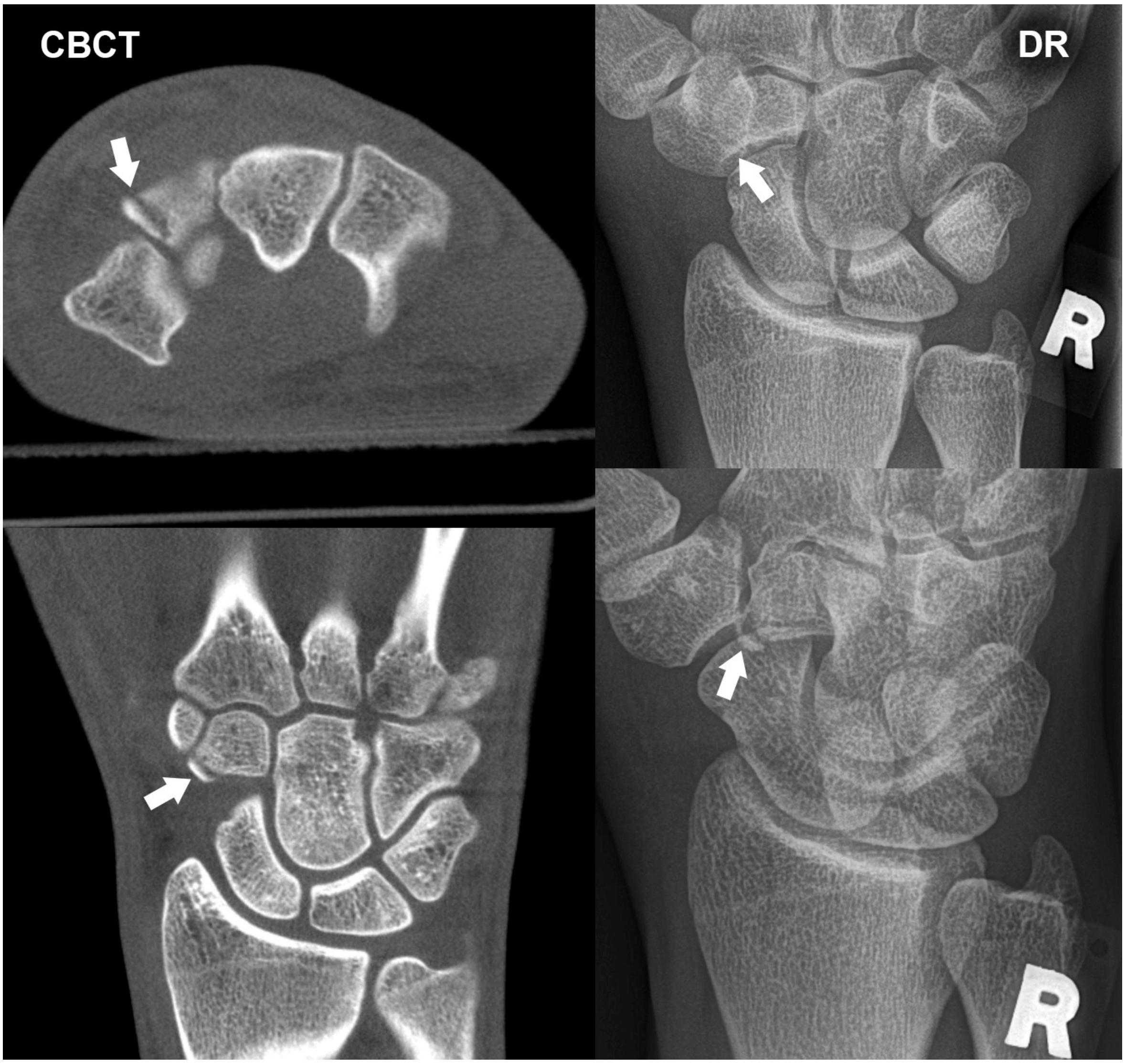

Figure 17. Imaging of the wrist of a 17-year-old adolescent with a fracture of the trapezoid bone. The fracture was seen on CBCT, but only seen on a second-look in DR.

Overall, most of the presented studies cover special aspects of the novel extremity CBCT devices or report initial experiences. In the majority, they suffer from a lack of included patients. Therefore, further evaluations are inevitable.

4.1.3. Review literature

Review literature and meta-analyses on extremity CBCT in children are practically non-existent to date. The authors of a general review article on CBCT (extremity, cervical spine, pyramids, paranasal sinuses) stated that “the effective dose varied considerably” in the studies evaluated, which was caused by a variety of different scanners and scanning protocols. They also pointed out that they were not able to perform a proper meta-analysis based on the currently available literature and added that further studies would be necessary (88).

4.2. Radiation dose considerations

Studies dealing with an increased risk for cancer development caused by ionizing radiation in childhood attracted big attention within the scientific community lately (10, 12, 154). There is an ongoing debate, whether and to what degree the published results were biased by underlying diseases (10, 154) or a referrer’s clinical questions (155). Anyhow, low-dose ionizing radiation seems to be a significant factor for excess cancer in later life.

Regarding extremity CT, decreasing radiation sensitivity is assumed, the further a scanned region is away from the trunk (156, 157). This concept may be well-established in grown-ups but could be wrong in children. The main factor of uncertainty in this regard remains the distribution of yellow and red bone marrow, which varies at different ages and between individuals (158-160). An ongoing debate in pediatric radiology is the establishment of proper tissue conversion factors as the basis for radiation dose risk using effective dose (161). We, therefore, tried to avoid the use of effective doses in this manuscript, as too many unknowns impair a robust estimation. Based on the currently available tissue weighting factors by the International Commission on Radiological Protection (ICRP) (162, 163), MDCT and CBCT examinations were calculated to be between 0.2 to 0.3 mSv on average, which equals 4 to 5 days of natural background radiation of worldwide 2.4 mSv (164).

The initially assumed exceptionally low doses of extremity CBCT (18) were not confirmed by later studies (21, 140, 165). The discrepancy is causally determined by an unrealistic study setting, comparing optimized CBCT with a quite old MDCT scanner without special optimizations (18).

Studies demonstrate that traumatized children undergoing CT should be scanned at specialized pediatric centers, or the examinations should at least be performed with optimized pediatric exposure protocols. Otherwise, they receive about double the dose unnecessarily (166, 167).

The increasing awareness of radiation-related risks lead to the initiation of various dose reduction campaigns, with the most prominent member "Image Gently®" under the patronage of the Society for Pediatric Radiology (SPR), the American Association of Physicists in Medicine (AAPM), the American College of Radiology (ACR), and the American Society of Radiologic Technologists (ASRT) (168-174). In the context of dose reduction programs, the term ALARA (as low as reasonably achievable) is often used, known since 1912 (175-178).

4.3. Image quality-related aspects

Image quality and dose are inextricably linked with each other in CBCT and MDCT (179). When dose settings are lowered, fewer X-ray quanta reach the detector with the result of increased image noise. Apart from noise, also contrast depends on the chosen exposure settings, where lower kVp options increase the contrast of high-density tissues with the drawback of increased scatter. The size of the detector elements determines the maximum resolution (101).

Apart from these main image quality factors, artifacts influence image quality to various degrees (117). In our study, the different types of artifacts where typically seen either in CBCT or in MDCT. Beam hardening artifacts and occasionally motion artifacts were observed in CBCT, where the latter can be explained by the longer acquisition time of more than half a minute in CBCT. In contrast, aliasing artifacts were a domain of MDCT.

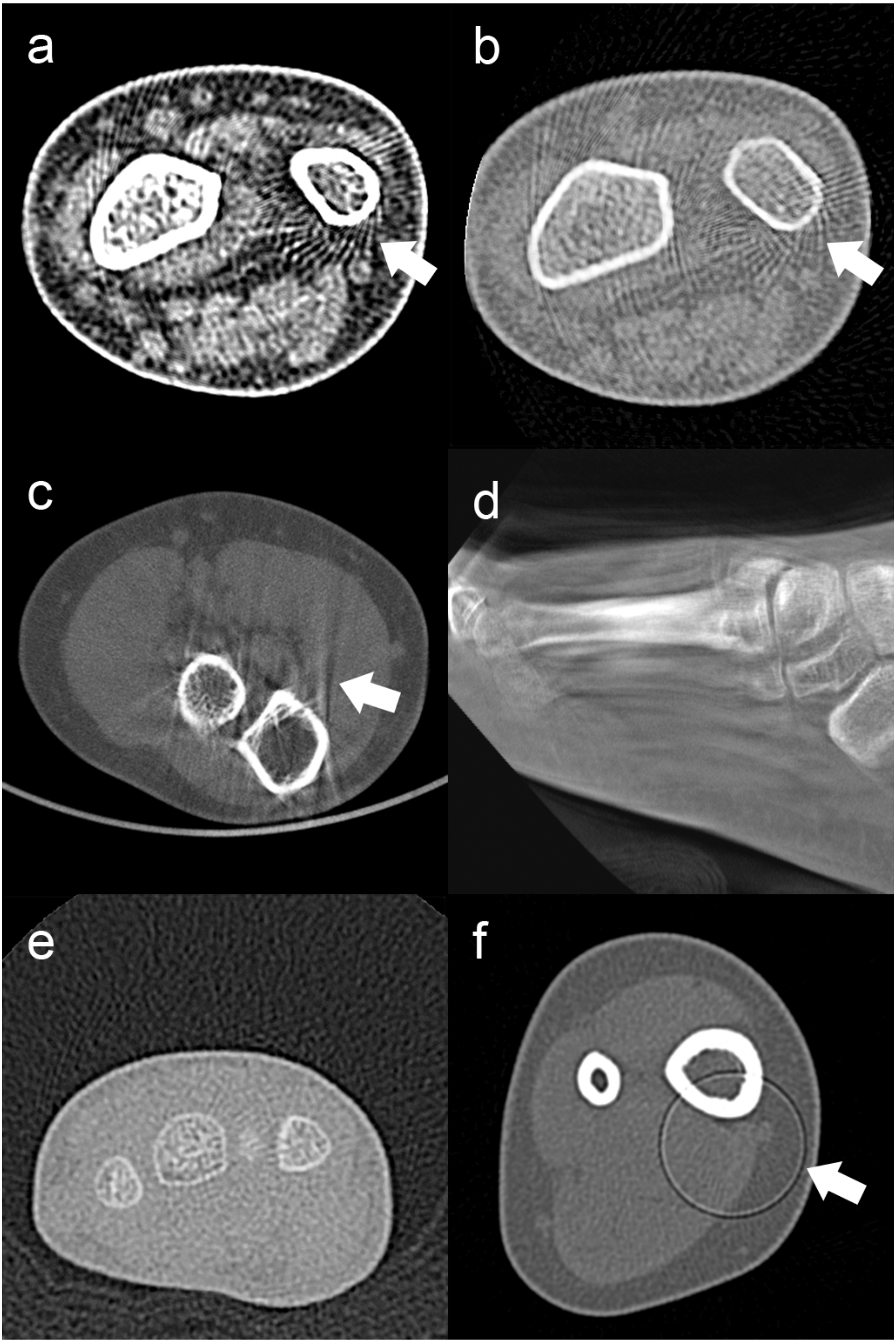

Figure 18. Examples of typical artifacts observed in CT examinations.

Aliasing artifact in a and b (MDCT), streak artifacts in c (CBCT), motion artifacts in d (CBCT), noise in e (MDCT), and a ring artifact in f (MDCT).

4.3.1. Greyscale values in CBCT

It is a known issue that CBCT gray levels vary more severely than in MDCT, from subject to subject, scanner to scanner (180-182), exposure protocol to exposure protocol (183), and especially when compared between both modalities (134, 184). A dependency between HU values and kVp is well known in the literature (166, 185). A study on phantoms reported that the tested CBCT devices did not show accurate tissue densities, which was independent of the acquisition parameters, tissue thickness, and location of an object within the examined phantom (132). Another related study on human mandibles found that reliability of grayscale measurements between CBCT and MDCT was insufficient in high-density structures, like cortical bone, and more accurate in low-density (hypodense) areas (136), which was also observed in this work. Special calibration methods to overcome the shortcomings of inaccurate CBCT gray values in dense structures were proposed by Liu et al., using an attenuation ratio between two adjacent tissues like bone and muscle for error correction, also lacking the need for additional hardware equipment (135). Anyway, the influence of the software used to measure these grayscale values itself seems to be negligible and measurements done by different software solutions should be approximately similar (184).

4.3.2. Soft tissue visualization

CT is generally not the method of choice in pediatric extremity soft tissue imaging, due to capable alternatives like ultrasound and MRI. Important findings like soft tissue swellings, hematomas, and air inclusions are readily detectable in most CT studies, while other soft tissue injuries usually stay occult. The observers assigned low ratings of soft tissue recognizability in both devices. Some CBCT and MDCT machines offer dual energy options, which would allow to asses soft tissues in more detail and enable to visualize bone marrow edema (186). We could not conduct dual energy studies, neither in CBCT nor in MDCT.

4.3.3. Iterative reconstruction

For many decades, CT images were reconstructed with the filtered back projection (FBP) method. Today, iterative reconstruction (IR) algorithms are standard in modern MDCT scanners, mainly implemented as adaptive statistical iterative reconstruction (ASIR) and as model-based iterative reconstruction (MBIR) (187, 188). ASIR was the first generation of IR, often described as hybrid IR, while the newer MBIR, or pure IR, is believed to be superior, but also more computational-intensive (189). The Toshiba Aquilion One MDCT assessed in this dissertation manuscript was upgraded with ASIR [referred explicitly to “AIDR3D” by the manufacturer (2, 190)] in 2012. Our data in this regard showed a significant drop in radiation dose after the rollout. This substantial dose reduction conforms with the available literature on this topic (187, 188, 191-194). One related study by Shah et al. examined the impact of IR in pediatric lower extremity MDCT. Dose reductions of 24-34% were reported. The authors concluded that noise levels were superior with activated IR, whereas measured and rated image quality decreased to some extent. They suggested to discuss and weigh the advantages and disadvantages in the respective institutions, and stated that further research would be necessary (195). In the local Pediatric Radiology Division, we routinely enable IR in the vast majority of the performed MDCT examinations, as recommended in the literature (166, 190, 193).

Different IR reconstruction algorithms are developed for CBCT and have been proposed in the literature (162-166). An IR algorithm was also implemented in the Planmed Verity CBCT as “Ultra Low Dose (ULD)” imaging protocol lately, approved by the FDA in 2018 (196). Our test sample was not yet equipped with the IR algorithm, so we could not review the possible benefits of the novel reconstruction technique in CBCT.

4.3.4. Scout images

Radiological technologists typically do scout views (pilot scan, topograms, survey views) of regions to be scanned with an MDCT. These consist of one or two topogram images to assist in planning an examination and are the basis for modulating tube current. There are no reports in the literature, to what degree scout images increase radiation dose in extremity CT examinations. However, a study on chest CT scout images showed relevant doses, especially if not optimized (197). As extremity scans can be acquired with region- and age-dependent fixed tube voltages and current settings, scout images are not required at all. Like in CBCT, MDCTs can be performed by positioning the injured body part by reference to laser position markers, available on many scanners. In a worst-case scenario, using automatic tube current (and kilovoltage) mechanisms could lead to unnecessarily high exposures, specifically if radiopaque structures are present in the scan field that misguide the dose setting algorithms (198). Taking all these criteria into account, we would generally recommend to stick with static exposure presets, adapted to patient age.

4.4. CBCT-specific features

4.4.1. Device mobility

Manufacturers equipped the currently available dedicated CBCT scanners with wheels, which together with compact form factors allow relocatability. However, this mobility could be less valuable than one might think in the first moment, mainly due to two reasons: Firstly, the devices are still bulky and weigh a few hundred kilograms. Movement is therefore not convenient, and transportation attempts make the sophisticated devices prone to mechanical damaging. Secondly, local regulations may require a shielded site to allow operation, requiring a specific radiation protected facility or room and rendering the whole feature void. Especially in a hospital environment, it is likely that an operator will use the mobility feature only on rare occasions or never. Thus, we believe that the mobility potential is preferably to be used in an ambulatory setting.

4.4.2. Weight-bearing

A majority of dedicated extremity CBCT devices offer the possibility to perform examinations of the leg, specifically the joints of the foot, the ankle, and the knee, under weight-bearing (WB) (14, 82, 83, 125). In adults, studies addressed the weight-bearing specific properties in the ankle (82, 126, 199-201), the foot (81, 84-86), and the knee (80, 87, 202), with the majority of them reporting a piece of additional diagnostic information. No particular studies were published in children. In the context of pediatric fractures, the application of weight-bearing CBCT appears to be relatively small, and we did not conduct weight-bearing experiments in this manuscript.

4.4.3. Lead curtain shield

The CBCT used in this study was optionally equipped with a lead curtain shield that, when mounted, separated the greater part of the examined extremity from the rest of the patient. A study reported this shielding to minimize the scatter radiation to the patient effectively (169). Radiological technologists applied this shielding whenever possible, and also used lead coverings in MDCT, when feasible to do so.

4.5. Limitations

Some limitations interfere with the results of this study and therefore need to be discussed in greater detail. The most important constraint is the small number of patients that we were able to recruit prospectively, specifically concerning the parallelly acquired CBCTs and MDCTs with only ten examination pairs. Small sample sizes are a common drawback in studies involving pediatric patients (203, 204). The second major weakness of the current manuscript is caused by technical differences between CBCT and MDCT, which render a reliable comparison of the images' gray levels impossible. We tried to overcome this drawback by correcting the grayscale values of the CBCT by directly referencing them to HU of the MDCTs performed in parallel. Another issue is caused by the selection of the exposure protocols in both devices, as they can be considered chosen haphazardly. The choice of the exposure settings was based on our long-term experience in musculoskeletal CT and pre-study testing on cadavers and phantoms, with the goal to achieve a balance of dose and noise. It needs to be stated that many settings would have changed the visual appearance of the studies, for example when lowering kVp from 100 to 120 in MDCT, using different reconstruction kernels or disabling iterative reconstruction. Despite all these unknowns, we decided to compare the devices and did this as realistically as we could. It should also be mentioned that a complete blinded reading of the examinations was impossible, as the devices display specific types of image characteristics and artifacts, revealing the underlying modality to the rater. We also did not record study durations and patient comfort during CBCT and MDCT, where the latter due to more comfortable positioning is potentially beneficial in CBCT when imaging elbow joints. Both aspects would warrant further research.

5. Conclusions

Dedicated pediatric extremity CBCT offers superior semi-objective image quality characteristics over corresponding MDCT. On the other hand, subjective image quality and diagnostic certainty are rated inferior in CBCT, mainly due to streak artifacts. There also is a little susceptibility to motion artifacts in CBCT. From a radiation protection perspective, neither extremity CBCT nor MDCT is of real concern in a pediatric trauma setting, as incidence is low when thoroughly-indicated and doses of one examination equal only a few days of natural background radiation.

Bibliography

1. Sorantin E, Weissensteiner S, Hasenburger G, Riccabona M. CT in children--dose protection and general considerations when planning a CT in a child. European journal of radiology. 2013;82(7):1043-9.

2. Sorantin E, Riccabona M, Stucklschweiger G, Guss H, Fotter R. Experience with volumetric (320 rows) pediatric CT. European journal of radiology. 2013;82(7):1091-7.

3. Imerci A, Canbek U, Kaya A, Sürer L, Savran A. Distribution of occult fractures detected in emergency orthopedic patient trauma with computerized tomography. Ulus Travma Acil Cerrahi Derg. 2013;19(2):157-63.

4. Cheng Z, Wang X, Duan Y, Wu L, Wu D, Chao B, et al. Low-dose prospective ECG-triggering dual-source CT angiography in infants and children with complex congenital heart disease: first experience. European radiology. 2010;20(10):2503-11.

5. Sanchez Jacob R, Vano-Galvan E, Vano E, Gomez Ruiz N, Fernandez Soto JM, Martinez Barrio D, et al. Optimising the use of computed radiography in pediatric chest imaging. Journal of digital imaging. 2009;22(2):104-13.

6. Berland LL, Smith JK. Multidetector-array CT: once again, technology creates new opportunities. Radiology. 1998;209(2):327-9.

7. Weg N, Scheer MR, Gabor MP. Liver lesions: improved detection with dual-detector-array CT and routine 2.5-mm thin collimation. Radiology. 1998;209(2):417-26.

8. Jarvinen H, Seuri R, Kortesniemi M, Lajunen A, Hallinen E, Savikurki-Heikkila P, et al. Indication-based national diagnostic reference levels for paediatric CT: a new approach with proposed values. Radiation protection dosimetry. 2015;165(1-4):86-90.

9. Muhm M, Danko T, Henzler T, Luiz T, Winkler H, Ruffing T. Pediatric trauma care with computed tomography--criteria for CT scanning. Emerg Radiol. 2015;22(6):613-21.

10. Berrington de Gonzalez A, Salotti JA, McHugh K, Little MP, Harbron RW, Lee C, et al. Relationship between paediatric CT scans and subsequent risk of leukaemia and brain tumours: assessment of the impact of underlying conditions. Br J Cancer. 2016;114(4):388-94.

11. Journy N, Rehel JL, Ducou Le Pointe H, Lee C, Brisse H, Chateil JF, et al. Are the studies on cancer risk from CT scans biased by indication? Elements of answer from a large-scale cohort study in France. Br J Cancer. 2015;112(1):185-93.

12. Mathews JD, Forsythe AV, Brady Z, Butler MW, Goergen SK, Byrnes GB, et al. Cancer risk in 680,000 people exposed to computed tomography scans in childhood or adolescence: data linkage study of 11 million Australians. BMJ (Clinical research ed). 2013;346:f2360.

13. Pearce MS, Salotti JA, Little MP, McHugh K, Lee C, Kim KP, et al. Radiation exposure from CT scans in childhood and subsequent risk of leukaemia and brain tumours: a retrospective cohort study. Lancet. 2012;380(9840):499-505.

14. Carrino JA, Al Muhit A, Zbijewski W, Thawait GK, Stayman JW, Packard N, et al. Dedicated cone-beam CT system for extremity imaging. Radiology. 2014;270(3):816-24.

15. Cao Q, Sisniega A, Brehler M, Stayman JW, Yorkston J, Siewerdsen JH, et al. Modeling and evaluation of a high-resolution CMOS detector for cone-beam CT of the extremities. Med Phys. 2018;45(1):114-30.

16. Koskinen SK, Haapamaki VV, Salo J, Lindfors NC, Kortesniemi M, Seppala L, et al. CT arthrography of the wrist using a novel, mobile, dedicated extremity cone-beam CT (CBCT). Skeletal radiology. 2013;42(5):649-57.

17. Koivisto J, Kiljunen T, Wolff J, Kortesniemi M. Assessment of effective radiation dose of an extremity CBCT, MSCT and conventional X ray for knee area using MOSFET dosemeters. Radiation protection dosimetry. 2013;157(4):515-24.

18. Koivisto J, Kiljunen T, Kadesjo N, Shi XQ, Wolff J. Effective radiation dose of a MSCT, two CBCT and one conventional radiography device in the ankle region. J Foot Ankle Res. 2015;8:8.

19. Matikka H, Viren T. Radiation dose reduction in cone-beam computed tomography of extremities: evaluation of a novel radiation shield. J Radiol Prot. 2014;34(2):N57-63.

20. Pugmire BS, Shailam R, Sagar P, Liu B, Li X, Palmer WE, et al. Initial Clinical Experience With Extremity Cone-Beam CT of the Foot and Ankle in Pediatric Patients. AJR American journal of roentgenology. 2016;206(2):431-5.

21. Tschauner S, Marterer R, Nagy E, Apfaltrer G, Riccabona M, Singer G, et al. Surface radiation dose comparison of a dedicated extremity cone beam computed tomography (CBCT) device and a multidetector computed tomography (MDCT) machine in pediatric ankle and wrist phantoms. PLoS One. 2017;12(6):e0178747.

22. Alamri HM, Sadrameli M, Alshalhoob MA, Sadrameli M, Alshehri MA. Applications of CBCT in dental practice: a review of the literature. Gen Dent. 2012;60(5):390-400; quiz 1-2.

23. Agrawal JM, Agrawal MS, Nanjannawar LG, Parushetti AD. CBCT in orthodontics: the wave of future. J Contemp Dent Pract. 2013;14(1):153-7.

24. Weber MT, Stratz N, Fleiner J, Schulze D, Hannig C. Possibilities and limits of imaging endodontic structures with CBCT. Swiss Dent J. 2015;125(3):293-311.

25. Hol C, Hellen-Halme K, Torgersen G, Nilsson M, Moystad A. How do dentists use CBCT in dental clinics? A Norwegian nationwide survey. Acta Odontol Scand. 2015;73(3):195-201.

26. Kapila SD, Nervina JM. CBCT in orthodontics: assessment of treatment outcomes and indications for its use. Dentomaxillofac Radiol. 2015;44(1):20140282.

27. Horner K, O'Malley L, Taylor K, Glenny AM. Guidelines for clinical use of CBCT: a review. Dentomaxillofac Radiol. 2015;44(1):20140225.

28. Machado GL. CBCT imaging - A boon to orthodontics. Saudi Dent J. 2015;27(1):12-21.

29. Kiljunen T, Kaasalainen T, Suomalainen A, Kortesniemi M. Dental cone beam CT: A review. Phys Med. 2015;31(8):844-60.

30. Abuhaimed A, Martin CJ, Sankaralingam M, Gentle DJ. Investigation of practical approaches to evaluating cumulative dose for cone beam computed tomography (CBCT) from standard CT dosimetry measurements: a Monte Carlo study. Phys Med Biol. 2015;60(14):5413-38.

31. Buckley JG, Wilkinson D, Malaroda A, Metcalfe P. Investigation of the radiation dose from cone-beam CT for image-guided radiotherapy: A comparison of methodologies. Journal of applied clinical medical physics / American College of Medical Physics. 2018;19(1):174-83.

32. Hua C, Yao W, Kidani T, Tomida K, Ozawa S, Nishimura T, et al. A robotic C-arm cone beam CT system for image-guided proton therapy: design and performance. The British journal of radiology. 2017;90(1079):20170266.

33. Rankine L, Wan H, Parikh P, Maughan N, Poulsen P, DeWees T, et al. Cone-Beam Computed Tomography Internal Motion Tracking Should Be Used to Validate 4-Dimensional Computed Tomography for Abdominal Radiation Therapy Patients. Int J Radiat Oncol Biol Phys. 2016;95(2):818-26.

34. Ruschin M, Komljenovic PT, Ansell S, Menard C, Bootsma G, Cho YB, et al. Cone beam computed tomography image guidance system for a dedicated intracranial radiosurgery treatment unit. Int J Radiat Oncol Biol Phys. 2013;85(1):243-50.

35. Taniguchi T, Hara T, Shimozato T, Shiraki K, Ohono K, Maejima R. Influence of Acquisition Mode of Cone-beam Computed Tomography on Accuracy of Image Registration for Image-guided Radiotherapy. Nihon Hoshasen Gijutsu Gakkai Zasshi. 2017;73(8):646-53.

36. Cordemans V, Kaminski L, Banse X, Francq BG, Cartiaux O. Accuracy of a new intraoperative cone beam CT imaging technique (Artis zeego II) compared to postoperative CT scan for assessment of pedicle screws placement and breaches detection. Eur Spine J. 2017;26(11):2906-16.

37. Costa F, Tosi G, Attuati L, Cardia A, Ortolina A, Grimaldi M, et al. Radiation exposure in spine surgery using an image-guided system based on intraoperative cone-beam computed tomography: analysis of 107 consecutive cases. J Neurosurg Spine. 2016;25(5):654-9.

38. Erovic BM, Chan HH, Daly MJ, Pothier DD, Yu E, Coulson C, et al. Intraoperative cone-beam computed tomography and multi-slice computed tomography in temporal bone imaging for surgical treatment. Otolaryngol Head Neck Surg. 2014;150(1):107-14.

39. Hisano H, Sakuragi T, Kakiuchi Y, Takita S, Takeda Y, Morita S, et al. Usefulness of Intraoperative Cone Beam CT Images on Video-assisted Thoracic Surgery. Nihon Hoshasen Gijutsu Gakkai Zasshi. 2017;73(2):87-95.

40. Okamura A, Nakaoka M, Ohbayashi N, Yahara K, Nabika S. Intraoperative cone-beam computed tomography contributes to avoiding hypoglossal nerve palsy during transvenous embolization for dural arteriovenous fistula of the anterior condylar confluence. Interv Neuroradiol. 2016;22(5):584-9.

41. Pua U, Lim GH. Cone-Beam CT-Guided Vertebroplasty in a Patient With Vertebra Plana. AJR American journal of roentgenology. 2016;207(1):196-9.

42. Vandevenne JE, Peuskens D, Wijnen L, Wuyts J. Cone-beam CT to assess bony fusion following anterior cervical interbody fusion. Eur Spine J. 2016;25 Suppl 1:134-9.

43. Bagla S, Rholl KS, Sterling KM, van Breda A, Papadouris D, Cooper JM, et al. Utility of cone-beam CT imaging in prostatic artery embolization. J Vasc Interv Radiol. 2013;24(11):1603-7.

44. Chen R, Geschwind JF, Wang Z, Tacher V, Lin M. Quantitative assessment of lipiodol deposition after chemoembolization: comparison between cone-beam CT and multidetector CT. J Vasc Interv Radiol. 2013;24(12):1837-44.

45. Loffroy R, Lin M, Yenokyan G, Rao PP, Bhagat N, Noordhoek N, et al. Intraprocedural C-arm dual-phase cone-beam CT: can it be used to predict short-term response to TACE with drug-eluting beads in patients with hepatocellular carcinoma? Radiology. 2013;266(2):636-48.

46. Raj S, Irani FG, Tay KH, Tan BS. C-arm Cone Beam Computed Tomography: A New Tool in the Interventional Suite. Annals of the Academy of Medicine, Singapore. 2013;42(11):585-92.

47. Suk Oh J, Jong Chun H, Gil Choi B, Giu Lee H. Transarterial chemoembolization with drug-eluting beads in hepatocellular carcinoma: usefulness of contrast saturation features on cone-beam computed tomography imaging for predicting short-term tumor response. J Vasc Interv Radiol. 2013;24(4):483-9.

48. Lee IJ, Chung JW, Yin YH, Kim HC, Kim YI, Jae HJ, et al. Cone-beam CT hepatic arteriography in chemoembolization for hepatocellular carcinoma: angiographic image quality and its determining factors. J Vasc Interv Radiol. 2014;25(9):1369-79; quiz 79- e1.

49. Lee SM, Park CM, Lee KH, Bahn YE, Kim JI, Goo JM. C-arm cone-beam CT-guided percutaneous transthoracic needle biopsy of lung nodules: clinical experience in 1108 patients. Radiology. 2014;271(1):291-300.

50. Cazzato RL, Battistuzzi JB, Catena V, Grasso RF, Zobel BB, Schena E, et al. Cone-Beam Computed Tomography (CBCT) Versus CT in Lung Ablation Procedure: Which is Faster? Cardiovasc Intervent Radiol. 2015;38(5):1231-6.

51. Jaconi M, Pagni F, Vacirca F, Leni D, Corso R, Cortinovis D, et al. C-arm cone-beam CT-guided transthoracic lung core needle biopsy as a standard diagnostic tool: an observational study. Medicine (Baltimore). 2015;94(12):e698.

52. Kickuth R, Reichling C, Bley T, Hahn D, Ritter C. C-Arm Cone-Beam CT Combined with a New Electromagnetic Navigation System for Guidance of Percutaneous Needle Biopsies: Initial Clinical Experience. RoFo : Fortschritte auf dem Gebiete der Rontgenstrahlen und der Nuklearmedizin. 2015;187(7):569-76.

53. Kim H, Park CM, Lee SM, Goo JM. C-Arm Cone-Beam CT Virtual Navigation-Guided Percutaneous Mediastinal Mass Biopsy: Diagnostic Accuracy and Complications. European radiology. 2015;25(12):3508-17.

54. Lee IJ, Chung JW, Yin YH, Kim HC, Kim YI, Jae HJ, et al. Cone-Beam Computed Tomography (CBCT) Hepatic Arteriography in Chemoembolization for Hepatocellular Carcinoma: Performance Depicting Tumors and Tumor Feeders. Cardiovasc Intervent Radiol. 2015;38(5):1218-30.

55. Patil VV, Fischman AM, Patel RS, Kim E, Lookstein RA, Tabori NE, et al. GI hemorrhage arising from splenic artery: intraprocedure cone-beam CT as problem-solving tool to aide in safe catheterization of offending vessel. Clin Imaging. 2015;39(5):928-30.

56. Schernthaner RE, Chapiro J, Sahu S, Withagen P, Duran R, Sohn JH, et al. Feasibility of a Modified Cone-Beam CT Rotation Trajectory to Improve Liver Periphery Visualization during Transarterial Chemoembolization. Radiology. 2015;277(3):833-41.

57. Tornqvist P, Dias N, Sonesson B, Kristmundsson T, Resch T. Intra-operative cone beam computed tomography can help avoid reinterventions and reduce CT follow up after infrarenal EVAR. Eur J Vasc Endovasc Surg. 2015;49(4):390-5.

58. Ben-Shlomo A, Cohen D, Bruckheimer E, Bachar GN, Konstantinovsky R, Birk E, et al. Comparing Effective Doses During Image-Guided Core Needle Biopsies with Computed Tomography Versus C-Arm Cone Beam CT Using Adult and Pediatric Phantoms. Cardiovasc Intervent Radiol. 2016;39(5):732-9.

59. Hu J, Maybody M, Cao G, Wang X, Chen H, Zhu X, et al. Lipiodol retention pattern assessed by cone beam computed tomography during conventional transarterial chemoembolization of hepatocellular carcinoma: accuracy and correlation with response. Cancer Imaging. 2016;16(1):32.

60. Jiao D, Huang K, Wu G, Wang Y, Han X. Flat detector cone-beam CT-guided percutaneous needle biopsy of mediastinal lesions: preliminary experience. Radiol Med. 2016;121(10):769-79.

61. Kinoshita M, Takechi K, Iwamoto S, Takao S, Shirono R, Harada M. The usefulness of cone-beam computed tomography during chemoembolization of hepatocellular carcinomas fed exclusively by the cystic artery. Jpn J Radiol. 2016;34(11):747-53.

62. Kroes MW, van Strijen MJ, Braak SJ, Hoogeveen YL, de Lange F, Schultze Kool LJ. The Use of Laser Guidance Reduces Fluoroscopy Time for C-Arm Cone-Beam Computed Tomography-Guided Biopsies. Cardiovasc Intervent Radiol. 2016;39(9):1322-6.

63. McKay T, Ingraham CR, Johnson GE, Kogut MJ, Vaidya S, Padia SA. Cone-Beam CT with Fluoroscopic Overlay Versus Conventional CT Guidance for Percutaneous Abdominopelvic Abscess Drain Placement. J Vasc Interv Radiol. 2016;27(1):52-7.

64. Ronot M, Abdel-Rehim M, Hakime A, Kuoch V, Roux M, Chiaradia M, et al. Cone-Beam CT Angiography for Determination of Tumor-Feeding Vessels During Chemoembolization of Liver Tumors: Comparison of Conventional and Dedicated-Software Analysis. J Vasc Interv Radiol. 2016;27(1):32-8.

65. Rotolo N, Floridi C, Imperatori A, Fontana F, Ierardi AM, Mangini M, et al. Comparison of cone-beam CT-guided and CT fluoroscopy-guided transthoracic needle biopsy of lung nodules. European radiology. 2016;26(2):381-9.

66. Amano T, Sato M, Matsumaru Y, Sakuma H, Yoda S, Hamada Y. Intra-arterial Contrasted Cone-beam Computed Tomography Assessment of Vessels Distal from Occluded Site in Acute Ischemic Stroke with Major Vessel Occlusion. Neurol Med Chir (Tokyo). 2017;57(6):292-8.

67. Choi JW, Kim HC, Lee JH, Yu SJ, Cho EJ, Kim MU, et al. Cone Beam CT-Guided Chemoembolization of Probable Hepatocellular Carcinomas Smaller than 1 cm in Patients at High Risk of Hepatocellular Carcinoma. J Vasc Interv Radiol. 2017;28(6):795-803 e1.

68. Ishikawa T, Imai M, Owaki T, Sato H, Nozawa Y, Sano T, et al. Hemodynamic Changes on Cone-Beam Computed Tomography during Balloon-Occluded Transcatheter Arterial Chemoembolization Using Miriplatin for Hepatocellular Carcinoma: A Preliminary Study. Dig Dis. 2017;35(6):598-601.

69. Jiao D, Xie N, Wu G, Ren J, Han X. C-arm cone-beam computed tomography with stereotactic needle guidance for percutaneous adrenal biopsy: initial experience. Acta Radiol. 2017;58(5):617-24.

70. Jonczyk M, Chapiro J, Collettini F, Geisel D, Schnapauff D, Streitparth F, et al. Diagnostic Accuracy of Split-Bolus Single-Phase Contrast-Enhanced Cone-Beam CT for the Detection of Liver Tumors before Transarterial Chemoembolization. J Vasc Interv Radiol. 2017;28(10):1378-85.

71. Kroes MW, Busser WM, Hoogeveen YL, de Lange F, Schultze Kool LJ. Laser Guidance in C-Arm Cone-Beam CT-Guided Radiofrequency Ablation of Osteoid Osteoma Reduces Fluoroscopy Time. Cardiovasc Intervent Radiol. 2017;40(5):728-34.

72. Minami Y, Takita M, Tsurusaki M, Yagyu Y, Ueshima K, Murakami T, et al. Semiquantitative prediction of early response of conventional transcatheter arterial chemoembolization for hepatocellular carcinoma using postprocedural plain cone-beam computed tomography. Hepatol Res. 2017;47(3):E113-E9.

73. Ogo T, Fukuda T, Tsuji A, Fukui S, Ueda J, Sanda Y, et al. Efficacy and safety of balloon pulmonary angioplasty for chronic thromboembolic pulmonary hypertension guided by cone-beam computed tomography and electrocardiogram-gated area detector computed tomography. European journal of radiology. 2017;89:270-6.

74. Osgood GM, Thawait GK, Hafezi-Nejad N, Shakoor D, Shaner A, Yorkston J, et al. Image quality of cone beam computed tomography for evaluation of extremity fractures in the presence of metal hardware: visual grading characteristics analysis. The British journal of radiology. 2017;90(1073):20160539.

75. Perry BC, Monroe EJ, McKay T, Kanal KM, Shivaram G. Pediatric Percutaneous Osteoid Osteoma Ablation: Cone-Beam CT with Fluoroscopic Overlay Versus Conventional CT Guidance. Cardiovasc Intervent Radiol. 2017;40(10):1593-9.

76. Wienbeck S, Lotz J, Fischer U. Feasibility of Vacuum-Assisted Breast Cone-Beam CT-Guided Biopsy and Comparison With Prone Stereotactic Biopsy. AJR American journal of roentgenology. 2017;208(5):1154-62.

77. Cornelis FH, Borgheresi A, Petre EN, Santos E, Solomon SB, Brown K. Hepatic Arterial Embolization Using Cone Beam CT with Tumor Feeding Vessel Detection Software: Impact on Hepatocellular Carcinoma Response. Cardiovasc Intervent Radiol. 2018;41(1):104-11.

78. Ludemann WM, Boning G, Chapiro J, Jonczyk M, Geisel D, Schnapauff D, et al. C-Arm Cone Beam CT for Intraprocedural Image Fusion and 3D Guidance in Portal Vein Embolization (PVE). Cardiovasc Intervent Radiol. 2018;41(3):424-32.

79. Weaver JJ, Natarajan N, Shaw DWW, Apkon SD, Koo KSH, Shivaram GM, et al. Transforaminal intrathecal delivery of nusinersen using cone-beam computed tomography for children with spinal muscular atrophy and extensive surgical instrumentation: early results of technical success and safety. Pediatric radiology. 2018;48(3):392-7.

80. Thawait GK, Demehri S, AlMuhit A, Zbijweski W, Yorkston J, Del Grande F, et al. Extremity cone-beam CT for evaluation of medial tibiofemoral osteoarthritis: Initial experience in imaging of the weight-bearing and non-weight-bearing knee. European journal of radiology. 2015;84(12):2564-70.

81. Collan L, Kankare JA, Mattila K. The biomechanics of the first metatarsal bone in hallux valgus: a preliminary study utilizing a weight bearing extremity CT. Foot Ankle Surg. 2013;19(3):155-61.

82. Ludlow JB, Ivanovic M. Weightbearing CBCT, MDCT, and 2D imaging dosimetry of the foot and ankle. International Journal of Diagnostic Imaging. 2014;1(2):1-9.

83. Tuominen EK, Kankare J, Koskinen SK, Mattila KT. Weight-bearing CT imaging of the lower extremity. AJR American journal of roentgenology. 2013;200(1):146-8.

84. de Cesar Netto C, Schon LC, Thawait GK, da Fonseca LF, Chinanuvathana A, Zbijewski WB, et al. Flexible Adult Acquired Flatfoot Deformity: Comparison Between Weight-Bearing and Non-Weight-Bearing Measurements Using Cone-Beam Computed Tomography. The Journal of bone and joint surgery American volume. 2017;99(18):e98.

85. Colin F, Horn Lang T, Zwicky L, Hintermann B, Knupp M. Subtalar joint configuration on weightbearing CT scan. Foot Ankle Int. 2014;35(10):1057-62.

86. Hirschmann A, Pfirrmann CW, Klammer G, Espinosa N, Buck FM. Upright cone CT of the hindfoot: comparison of the non-weight-bearing with the upright weight-bearing position. European radiology. 2014;24(3):553-8.

87. Halonen KS, Mononen ME, Jurvelin JS, Toyras J, Salo J, Korhonen RK. Deformation of articular cartilage during static loading of a knee joint--experimental and finite element analysis. Journal of biomechanics. 2014;47(10):2467-74.

88. Nardi C, Salerno S, Molteni R, Occhipinti M, Grazzini G, Norberti N, et al. Radiation dose in non-dental cone beam CT applications: a systematic review. Radiol Med. 2018.

89. Shaw CC. Cone Beam Computed Tomography. Philadelphia: CRC Press; 2014. 1 online resource (266 pages) p.

90. Wood EH. Noninvasive three-dimensional viewing of the motion and anatomical structure of the heart, lungs, and circulatory system by high speed computerized X-ray tomography. CRC Crit Rev Biochem. 1979;7(2):161-86.

91. Scanlan JG, Gustafson DE, Chevalier PA, Robb RA, Ritman EL. Evaluation of ischemic heart disease with a prototype volume imaging computed tomographic (CT) scanner: preliminary experiments. The American journal of cardiology. 1980;46(7):1263-8.

92. Robb RA, Lent AH, Gilbert BK, Chu A. The dynamic spatial reconstructor: a computed tomography system for high-speed simultaneous scanning of multiple cross sections of the heart. J Med Syst. 1980;4(2):253-88.

93. Ritman EL, Kinsey JH, Robb RA, Gilbert BK, Harris LD, Wood EH. Three-dimensional imaging of heart, lungs, and circulation. Science. 1980;210(4467):273-80.

94. Ritman EL, Harris LD, Kinsey JH, Robb RA. Computed tomographic imaging of the heart: the dynamic spatial reconstructor. Radiologic clinics of North America. 1980;18(3):547-55.

95. Robb RA, A. HE, Sinak LJ, Harris LD, Ritman EL. High-speed three-dimensional X-ray computed tomography: The dynamic spatial reconstructor. Proceedings of the IEEE. 1983;71(3):308-19.

96. Mozzo P, Procacci C, Tacconi A, Martini PT, Andreis IA. A new volumetric CT machine for dental imaging based on the cone-beam technique: preliminary results. European radiology. 1998;8(9):1558-64.

97. Ludlow JB, Davies-Ludlow LE, Brooks SL. Dosimetry of two extraoral direct digital imaging devices: NewTom cone beam CT and Orthophos Plus DS panoramic unit. Dentomaxillofac Radiol. 2003;32(4):229-34.

98. Erickson M, Caruso JM, Leggitt L. Newtom QR-DVT 9000 imaging used to confirm a clinical diagnosis of iatrogenic mandibular nerve paresthesia. J Calif Dent Assoc. 2003;31(11):843-5.

99. Mah JK, Danforth RA, Bumann A, Hatcher D. Radiation absorbed in maxillofacial imaging with a new dental computed tomography device. Oral Surg Oral Med Oral Pathol Oral Radiol Endod. 2003;96(4):508-13.

100. Tang X, Krupinski EA, Xie H, Stillman AE. On the data acquisition, image reconstruction, cone beam artifacts, and their suppression in axial MDCT and CBCT - A review. Med Phys. 2018.

101. Kalender W. Computed tomography : fundamentals, system technology, image quality, applications. 3rd ed. Erlangen: Publicis Publishing; 2011. 372 p.

102. Kyriakou Y, Kalender W. Efficiency of antiscatter grids for flat-detector CT. Phys Med Biol. 2007;52(20):6275-93.

103. Kalender WA, Kyriakou Y. Flat-detector computed tomography (FD-CT). European radiology. 2007;17(11):2767-79.

104. Kyriakou Y, Meyer M, Kalender WA. Technical note: comparing coherent and incoherent scatter effects for cone-beam CT. Physics in medicine and biology. 2008;53(10):N175-85.

105. Wang B, Liu H, Zhao S, Wang G. Feldkamp-type image reconstruction from equiangular data. J Xray Sci Technol. 2001;9(3):113-20.

106. Jin JY, Ren L, Liu Q, Kim J, Wen N, Guan H, et al. Combining scatter reduction and correction to improve image quality in cone-beam computed tomography (CBCT). Med Phys. 2010;37(11):5634-44.

107. Lechuga L, Weidlich GA. Cone Beam CT vs. Fan Beam CT: A Comparison of Image Quality and Dose Delivered Between Two Differing CT Imaging Modalities. Cureus. 2016;8(9):e778.

108. Nagarajappa AK, Dwivedi N, Tiwari R. Artifacts: The downturn of CBCT image. J Int Soc Prev Community Dent. 2015;5(6):440-5.

109. Pengpan T, Smith ND, Qiu W, Yao A, Mitchell CN, Soleimani M. A motion-compensated cone-beam CT using electrical impedance tomography imaging. Physiol Meas. 2011;32(1):19-34.

110. Siewerdsen JH, Jaffray DA. Cone-beam computed tomography with a flat-panel imager: magnitude and effects of x-ray scatter. Med Phys. 2001;28(2):220-31.

111. Makins SR. Artifacts interfering with interpretation of cone beam computed tomography images. Dent Clin North Am. 2014;58(3):485-95.

112. Liu Y, Liu H, Wang Y, Wang G. Half-scan cone-beam CT fluoroscopy with multiple x-ray sources. Med Phys. 2001;28(7):1466-71.

113. Miracle AC, Mukherji SK. Conebeam CT of the head and neck, part 1: physical principles. AJNR Am J Neuroradiol. 2009;30(6):1088-95.

114. Feldkamp LA, Davis LC, Kress JW. Practical cone-beam algorithm. JOSA. 1984;1(6):612-9.

115. Mosby I. Mosby's medical dictionary. 8th ed. St. Louis, Mo.: Mosby; 2009. p. p.

116. Dorland WAN. Dorland's illustrated medical dictionary. 31st ed. Philadelphia, PA: Saunders; 2007. xxvii, 2175 p. p.

117. Barrett JF, Keat N. Artifacts in CT: recognition and avoidance. Radiographics. 2004;24(6):1679-91.

118. Mori I, Machida Y, Osanai M, Iinuma K. Photon starvation artifacts of X-ray CT: their true cause and a solution. Radiol Phys Technol. 2013;6(1):130-41.

119. Bastos M, Lee EY, Strauss KJ, Zurakowski D, Tracy DA, Boiselle PM. Motion artifact on high-resolution CT images of pediatric patients: comparison of volumetric and axial CT methods. AJR American journal of roentgenology. 2009;193(5):1414-8.

120. Sisniega A, Stayman JW, Cao Q, Yorkston J, Siewerdsen JH, Zbijewski W. Image-Based Motion Compensation for High-Resolution Extremities Cone-Beam CT. Proc SPIE Int Soc Opt Eng. 2016;9783.

121. Sisniega A, Stayman JW, Yorkston J, Siewerdsen JH, Zbijewski W. Motion compensation in extremity cone-beam CT using a penalized image sharpness criterion. Phys Med Biol. 2017;62(9):3712-34.

122. Ouadah S, Jacobson M, Stayman JW, Ehtiati T, Weiss C, Siewerdsen JH. Correction of patient motion in cone-beam CT using 3D-2D registration. Phys Med Biol. 2017;62(23):8813-31.

123. Artul S. Ring artefact in multidetector CT. BMJ Case Rep. 2013;2013.

124. Mithun S, Jha AK, Panchal K, Purandare NC, Shah S, Agrawal A, et al. A rare cause of tube arcing artifact seen in computed tomography image of a positron emission tomography/computed tomography scanner. Indian J Radiol Imaging. 2016;26(1):153-5.

125. Zbijewski W, De Jean P, Prakash P, Ding Y, Stayman JW, Packard N, et al. A dedicated cone-beam CT system for musculoskeletal extremities imaging: design, optimization, and initial performance characterization. Med Phys. 2011;38(8):4700-13.

126. Lintz F, de Cesar Netto C, Barg A, Burssens A, Richter M, Weight Bearing CTISG. Weight-bearing cone beam CT scans in the foot and ankle. EFORT Open Rev. 2018;3(5):278-86.

127. Koivisto J, Schulze D, Wolff J, Rottke D. Effective dose assessment in the maxillofacial region using thermoluminescent (TLD) and metal oxide semiconductor field-effect transistor (MOSFET) dosemeters: a comparative study. Dentomaxillofac Radiol. 2014;43(8):20140202.

128. Kern M, Tucker A, Rogers K, Kruse RW. CT Utilization for Pediatric Orthopedic Trauma. Del Med J. 2015;87(12):366-9.

129. O'Dell MC, Jaramillo D, Bancroft L, Varich L, Logsdon G, Servaes S. Imaging of Sports-related Injuries of the Lower Extremity in Pediatric Patients. Radiographics. 2016;36(6):1807-27.

130. Delgado J, Jaramillo D, Chauvin NA. Imaging the Injured Pediatric Athlete: Upper Extremity. Radiographics. 2016;36(6):1672-87.

131. Lee CH, Ryu JH, Lee YH, Yoon KH. Reduction of radiation exposure by lead curtain shielding in dedicated extremity cone beam CT. The British journal of radiology. 2015;88(1050):20140866.

132. Kyoto Kagaku. Pediatric Whole Body Phantom "PBU-70" Kitanekoya-cho Fushimi-ku Kyoto, Japan: Kyoto Kagaku Co., Ltd.,; 2016 [Available from: https://kyotokagaku.com/products/detail03/ph-2c.html.

133. Schindelin J, Arganda-Carreras I, Frise E, Kaynig V, Longair M, Pietzsch T, et al. Fiji: an open-source platform for biological-image analysis. Nature methods. 2012;9(7):676-82.

134. Silva IM, Freitas DQ, Ambrosano GM, Boscolo FN, Almeida SM. Bone density: comparative evaluation of Hounsfield units in multislice and cone-beam computed tomography. Braz Oral Res. 2012;26(6):550-6.

135. Liu Y, Bauerle T, Pan L, Dimitrakopoulou-Strauss A, Strauss LG, Heiss C, et al. Calibration of cone beam CT using relative attenuation ratio for quantitative assessment of bone density: a small animal study. Int J Comput Assist Radiol Surg. 2013;8(5):733-9.

136. Patrick S, Birur NP, Gurushanth K, Raghavan AS, Gurudath S. Comparison of gray values of cone-beam computed tomography with hounsfield units of multislice computed tomography: An in vitro study. Indian J Dent Res. 2017;28(1):66-70.

137. Varshowsaz M, Goorang S, Ehsani S, Azizi Z, Rahimian S. Comparison of Tissue Density in Hounsfield Units in Computed Tomography and Cone Beam Computed Tomography. J Dent (Tehran). 2016;13(2):108-15.

138. Arisan V, Karabuda ZC, Avsever H, Ozdemir T. Conventional multi-slice computed tomography (CT) and cone-beam CT (CBCT) for computer-assisted implant placement. Part I: relationship of radiographic gray density and implant stability. Clin Implant Dent Relat Res. 2013;15(6):893-906.

139. Neubauer J, Neubauer C, Gerstmair A, Krauss T, Reising K, Zajonc H, et al. Comparison of the Radiation Dose from Cone Beam Computed Tomography and Multidetector Computed Tomography in Examinations of the Hand. RoFo : Fortschritte auf dem Gebiete der Rontgenstrahlen und der Nuklearmedizin. 2016.

140. Lang H, Neubauer J, Fritz B, Spira EM, Strube J, Langer M, et al. A retrospective, semi-quantitative image quality analysis of cone beam computed tomography (CBCT) and MSCT in the diagnosis of distal radius fractures. European radiology. 2016.

141. Edlund R, Skorpil M, Lapidus G, Backlund J. Cone-Beam CT in diagnosis of scaphoid fractures. Skeletal radiology. 2015.

142. Huang AJ, Chang CY, Thomas BJ, MacMahon PJ, Palmer WE. Using cone-beam CT as a low-dose 3D imaging technique for the extremities: initial experience in 50 subjects. Skeletal radiology. 2015;44(6):797-809.

143. Neubauer J, Benndorf M, Reidelbach C, Krauss T, Lampert F, Zajonc H, et al. Comparison of Diagnostic Accuracy of Radiation Dose-Equivalent Radiography, Multidetector Computed Tomography and Cone Beam Computed Tomography for Fractures of Adult Cadaveric Wrists. PLoS One. 2016;11(10):e0164859.

144. Neubauer J, Benndorf M, Ehritt-Braun C, Reising K, Yilmaz T, Klein C, et al. Comparison of the diagnostic accuracy of cone beam computed tomography and radiography for scaphoid fractures. Sci Rep. 2018;8(1):3906.

145. Andresen R, Radmer S, Sparmann M, Bogusch G, Banzer D. Imaging of hamate bone fractures in conventional X-rays and high-resolution computed tomography. An in vitro study. Investigative radiology. 1999;34(1):46-50.

146. de Zwart AD, Beeres FJ, Rhemrev SJ, Bartlema K, Schipper IB. Comparison of MRI, CT and bone scintigraphy for suspected scaphoid fractures. Eur J Trauma Emerg Surg. 2016;42(6):725-31.

147. Fotiadou A, Patel A, Morgan T, Karantanas AH. Wrist injuries in young adults: the diagnostic impact of CT and MRI. European journal of radiology. 2011;77(2):235-9.

148. Kato H, Nakamura R, Horii E, Nakao E, Yajima H. Diagnostic imaging for fracture of the hook of the hamate. Hand Surg. 2000;5(1):19-24.

149. Rhemrev SJ, de Zwart AD, Kingma LM, Meylaerts SA, Arndt JW, Schipper IB, et al. Early computed tomography compared with bone scintigraphy in suspected scaphoid fractures. Clin Nucl Med. 2010;35(12):931-4.

150. Takami M, Nohda K, Sakanaka J, Nakamura M, Yoshida M. Usefulness of full spine computed tomography in cases of high-energy trauma: a prospective study. Eur J Orthop Surg Traumatol. 2014;24 Suppl 1:S167-71.

151. Welling RD, Jacobson JA, Jamadar DA, Chong S, Caoili EM, Jebson PJ. MDCT and radiography of wrist fractures: radiographic sensitivity and fracture patterns. AJR American journal of roentgenology. 2008;190(1):10-6.

152. You JS, Chung SP, Chung HS, Park IC, Lee HS, Kim SH. The usefulness of CT for patients with carpal bone fractures in the emergency department. Emergency medicine journal : EMJ. 2007;24(4):248-50.

153. Shih CD, Bazarov I, Harrington T, Vartivarian M, Reyzelman AM. Initial Report on the Use of In-Office Cone Beam Computed Tomography for Early Diagnosis of Osteomyelitis in Diabetic Patients. J Am Podiatr Med Assoc. 2016;106(2):128-32.

154. Journy N, Roue T, Cardis E, Le Pointe HD, Brisse H, Chateil JF, et al. Childhood CT scans and cancer risk: impact of predisposing factors for cancer on the risk estimates. J Radiol Prot. 2016;36(1):N1-7.

155. Meulepas JM, Hauptmann M, Lubin JH, Shuryak I, Brenner DJ. Is there Unmeasured Indication Bias in Radiation-Related Cancer Risk Estimates from Studies of Computed Tomography? Radiation research. 2018;189(2):128-35.

156. Deak PD, Smal Y, Kalender WA. Multisection CT protocols: sex- and age-specific conversion factors used to determine effective dose from dose-length product. Radiology. 2010;257(1):158-66.

157. Saltybaeva N, Jafari ME, Hupfer M, Kalender WA. Estimates of effective dose for CT scans of the lower extremities. Radiology. 2014;273(1):153-9.

158. Ricci C, Cova M, Kang YS, Yang A, Rahmouni A, Scott WW, Jr., et al. Normal age-related patterns of cellular and fatty bone marrow distribution in the axial skeleton: MR imaging study. Radiology. 1990;177(1):83-8.

159. Vande Berg BC, Malghem J, Lecouvet FE, Maldague B. Magnetic resonance imaging of normal bone marrow. European radiology. 1998;8(8):1327-34.

160. Moore SG, Dawson KL. Red and yellow marrow in the femur: age-related changes in appearance at MR imaging. Radiology. 1990;175(1):219-23.

161. Newman B, Ganguly A, Kim JE, Robinson T. Comparison of different methods of calculating CT radiation effective dose in children. AJR American journal of roentgenology. 2012;199(2):W232-9.

162. Khong PL, Ringertz H, Donoghue V, Frush D, Rehani M, Appelgate K, et al. ICRP publication 121: Radiological protection in paediatric diagnostic and interventional radiology. Annals of the ICRP. 2013;42(2):1-63.

163. Valentin J, International Commission on Radiological Protection. ICRP publication 103: The 2007 Recommendations of the International Commission on Radiological

Protection. Amsterdam2007 [2007/12/18:[1-332]. Available from: http://www.ncbi.nlm.nih.gov/pubmed/18082557

https://ac.els-cdn.com/S0146645307000395/1-s2.0-S0146645307000395-main.pdf?_tid=9a1a21f8-c78b-43cd-8984-d71970eb3954&acdnat=1531476223_5d30601c3428951dfda22f64b53fce89.

164. United Nations Scientific Committee. Sources and effects of ionizing radiation : United Nations Scientific Committee on the Effects of Atomic Radiation : UNSCEAR 2008 Report to the General Assembly with Scientific Annexes. New York: United Nations; 2010.

165. Neubauer J, Voigt JM, Lang H, Scheuer C, Goerke SM, Langer M, et al. Comparing the image quality of a mobile flat-panel computed tomography and a multidetector computed tomography: a phantom study. Investigative radiology. 2014;49(7):491-7.

166. Greenwood TJ, Lopez-Costa RI, Rhoades PD, Ramirez-Giraldo JC, Starr M, Street M, et al. CT Dose Optimization in Pediatric Radiology: A Multiyear Effort to Preserve the Benefits of Imaging While Reducing the Risks. Radiographics. 2015;35(5):1539-54.

167. Nabaweesi R, Ramakrishnaiah RH, Aitken ME, Rettiganti MR, Luo C, Maxson RT, et al. Injured Children Receive Twice the Radiation Dose at Nonpediatric Trauma Centers Compared With Pediatric Trauma Centers. Journal of the American College of Radiology : JACR. 2018;15(1 Pt A):58-64.

168. Goske MJ, Charkot E, Herrmann T, John SD, Mills TT, Morrison G, et al. Image Gently: challenges for radiologic technologists when performing digital radiography in children. Pediatric radiology. 2011;41(5):611-9.

169. Moore QT, Don S, Goske MJ, Strauss KJ, Cohen M, Herrmann T, et al. Image gently: using exposure indicators to improve pediatric digital radiography. Radiologic technology. 2012;84(1):93-9.

170. Don S, Macdougall R, Strauss K, Moore QT, Goske MJ, Cohen M, et al. Image gently campaign back to basics initiative: ten steps to help manage radiation dose in pediatric digital radiography. AJR American journal of roentgenology. 2013;200(5):W431-6.

171. Goske MJ, Applegate KE, Boylan J, Butler PF, Callahan MJ, Coley BD, et al. The Image Gently campaign: working together to change practice. AJR American journal of roentgenology. 2008;190(2):273-4.

172. Dauer LT, St Germain J, Meyers PA. Let's image gently: reducing excessive reliance on CT scans. Pediatr Blood Cancer. 2008;51(6):838; author reply 9-40.

173. Goske MJ, Applegate KE, Boylan J, Butler PF, Callahan MJ, Coley BD, et al. Image Gently(SM): a national education and communication campaign in radiology using the science of social marketing. Journal of the American College of Radiology : JACR. 2008;5(12):1200-5.

174. Bulas D, Goske M, Applegate K, Wood B. Image Gently: improving health literacy for parents about CT scans for children. Pediatric radiology. 2009;39(2):112-6.

175. Winkler NT. ALARA concept--now a requirement. Radiologic technology. 1980;51(4):525.

176. Hendee WR, Edwards FM. ALARA and an integrated approach to radiation protection. Seminars in nuclear medicine. 1986;16(2):142-50.

177. Willis CE, Slovis TL. The ALARA concept in pediatric CR and DR: dose reduction in pediatric radiographic exams--a white paper conference. AJR American journal of roentgenology. 2005;184(2):373-4.

178. Oestreich AE. RSNA centennial article: ALARA 1912: "As low a dose as possible" a century ago. Radiographics. 2014;34(5):1457-60.

179. Goldman LW. Principles of CT: radiation dose and image quality. J Nucl Med Technol. 2007;35(4):213-25; quiz 26-8.

180. Lamba R, McGahan JP, Corwin MT, Li CS, Tran T, Seibert JA, et al. CT Hounsfield numbers of soft tissues on unenhanced abdominal CT scans: variability between two different manufacturers' MDCT scanners. AJR American journal of roentgenology. 2014;203(5):1013-20.

181. Ruder TD, Thali Y, Schindera ST, Dalla Torre SA, Zech WD, Thali MJ, et al. How reliable are Hounsfield-unit measurements in forensic radiology? Forensic science international. 2012;220(1-3):219-23.

182. Sande EP, Martinsen AC, Hole EO, Olerud HM. Interphantom and interscanner variations for Hounsfield units--establishment of reference values for HU in a commercial QA phantom. Phys Med Biol. 2010;55(17):5123-35.

183. Zurl B, Tiefling R, Winkler P, Kindl P, Kapp KS. Hounsfield units variations: impact on CT-density based conversion tables and their effects on dose distribution. Strahlenther Onkol. 2014;190(1):88-93.

184. Azeredo F, de Menezes LM, Enciso R, Weissheimer A, de Oliveira RB. Computed gray levels in multislice and cone-beam computed tomography. Am J Orthod Dentofacial Orthop. 2013;144(1):147-55.

185. Yu L, Bruesewitz MR, Thomas KB, Fletcher JG, Kofler JM, McCollough CH. Optimal tube potential for radiation dose reduction in pediatric CT: principles, clinical implementations, and pitfalls. Radiographics. 2011;31(3):835-48.

186. Zbijewski W, Sisniega A, Stayman JW, Thawait G, Packard N, Yorkston J, et al. Dual-Energy Imaging of Bone Marrow Edema on a Dedicated Multi-Source Cone-Beam CT System for the Extremities. Proc SPIE Int Soc Opt Eng. 2015;9412.

187. Kim HJ, Yoo SY, Jeon TY, Kim JH. Model-based iterative reconstruction in ultra-low-dose pediatric chest CT: comparison with adaptive statistical iterative reconstruction. Clin Imaging. 2016;40(5):1018-22.

188. Smith EA, Dillman JR, Goodsitt MM, Christodoulou EG, Keshavarzi N, Strouse PJ. Model-based iterative reconstruction: effect on patient radiation dose and image quality in pediatric body CT. Radiology. 2014;270(2):526-34.

189. Son SS, Choo KS, Jeon UB, Jeon GR, Nam KJ, Kim TU, et al. Image quality of CT angiography with model-based iterative reconstruction in young children with congenital heart disease: comparison with filtered back projection and adaptive statistical iterative reconstruction. Int J Cardiovasc Imaging. 2015;31 Suppl 1:31-8.

190. Didier RA, Vajtai PL, Hopkins KL. Iterative reconstruction technique with reduced volume CT dose index: diagnostic accuracy in pediatric acute appendicitis. Pediatric radiology. 2015;45(2):181-7.

191. Aurumskjold ML, Soderberg M, Stalhammar F, von Steyern KV, Tingberg A, Ydstrom K. Evaluation of an iterative model-based reconstruction of pediatric abdominal CT with regard to image quality and radiation dose. Acta Radiol. 2018;59(6):740-7.

192. Bae S, Kim MJ, Yoon CS, Kim DW, Hong JH, Lee MJ. Effects of adaptive statistical iterative reconstruction on radiation dose reduction and diagnostic accuracy of pediatric abdominal CT. Pediatric radiology. 2014;44(12):1541-7.

193. den Harder AM, Willemink MJ, Budde RP, Schilham AM, Leiner T, de Jong PA. Hybrid and model-based iterative reconstruction techniques for pediatric CT. AJR American journal of roentgenology. 2015;204(3):645-53.

194. Tilley S, 2nd, Siewerdsen JH, Stayman JW. Iterative CT Reconstruction using Models of Source and Detector Blur and Correlated Noise. Conf Proc Int Conf Image Form Xray Comput Tomogr. 2014;2014:363-7.

195. Shah A, Rees M, Kar E, Bolton K, Lee V, Panigrahy A. Adaptive statistical iterative reconstruction use for radiation dose reduction in pediatric lower-extremity CT: impact on diagnostic image quality. Skeletal radiology. 2018;47(6):785-93.

196. U.S. Food and Drug Administration (FDA). 510(k) Premarket Notification: K180918. Silver Spring, MD, USA: U.S. Food and Drug Administration; 2018.

197. O'Daniel JC, Stevens DM, Cody DD. Reducing radiation exposure from survey CT scans. AJR American journal of roentgenology. 2005;185(2):509-15.

198. Ryu YJ, Choi YH, Cheon JE, Park JE, Kim WS, Kim IO. Effect of arm position, presence of medical devices, and off-centering during acquisition of scout image on automatic tube voltage selection and current modulation in pediatric chest CT. PLoS One. 2018;13(4):e0195807.

199. Marzo JM, Kluczynski MA, Clyde C, Anders MJ, Mutty CE, Ritter CA. Weight bearing cone beam CT scan versus gravity stress radiography for analysis of supination external rotation injuries of the ankle. Quant Imaging Med Surg. 2017;7(6):678-84.

200. Lawlor MC, Kluczynski MA, Marzo JM. Weight-Bearing Cone-Beam CT Scan Assessment of Stability of Supination External Rotation Ankle Fractures in a Cadaver Model. Foot Ankle Int. 2018;39(7):850-7.

201. Shakoor D, Osgood GM, Brehler M, Zbijewski WB, de Cesar Netto C, Shafiq B, et al. Cone-beam CT measurements of distal tibio-fibular syndesmosis in asymptomatic uninjured ankles: does weight-bearing matter? Skeletal radiology. 2019;48(4):583-94.

202. Lam TC, Shrive NG, Frank CB. Variations in rupture site and surface strains at failure in the maturing rabbit medial collateral ligament. Journal of biomechanical engineering. 1995;117(4):455-61.

203. Duffett M, Choong K, Hartling L, Menon K, Thabane L, Cook DJ. Randomized controlled trials in pediatric critical care: a scoping review. Crit Care. 2013;17(5):R256.

204. Nikolakopoulos S, Roes KC, van der Lee JH, van der Tweel I. Sample size calculations in pediatric clinical trials conducted in an ICU: a systematic review. Trials. 2014;15:274.